# A sustainable framework for multi-microgrids energy management in automated distribution network by considering smart homes and high penetration of renewable energy resources

Mansouri Seyed Amir, Ahmarinejad Amir, Nematbakhsh Emad, Javadi Mohammad Sadegh, Esmaeel Nezhad Ali, Catalão João P. S.



**DOI:** 10.1016/j.energy.2022.123228

# A Sustainable Framework for Multi-Microgrids Energy Management in Automated Distribution Network by Considering Smart Homes and High Penetration of Renewable Energy Resources

S. A. Mansouri [1*], A. Ahmarinejad [2], E. Nematbakhsh [3], M. S. Javadi [4]
A. Esmaeel Nezhad [5] and J. P. S. Catalão[4,6]

[1] Department of Electrical Engineering, Yadegar-e-Imam Khomeini (RAH) Shahre Rey Branch, Islamic Azad University, Tehran, Iran
[2] Department of Electrical Engineering, Central Tehran Branch, Islamic Azad University, Tehran, Iran
[3] Faculty of Electrical Engineering, University of Isfahan, Isfahan, Iran
[4] Institute for Systems and Computer Engineering, Technology and Science (INESC TEC), Porto, Portugal
[5] Department of Electrical Engineering, School of Energy Systems, LUT University, 53850, Lappeenranta, Finland
[6] Faculty of Engineering of the University of Porto, Porto, Portugal

## Abstract

This paper presents a new framework for the scheduling of microgrids and distribution feeder reconfiguration (DFR), taking into consideration the uncertainties due to the load demand, market price, and renewable power generation. The model is implemented on the modified IEEE 118-bus test system, including microgrids and smart homes. The problem has been formulated as a two-stage model, which at the first stage, the day-ahead self-scheduling of each microgrid is carried out as a two-objective optimization problem. The two objectives include the minimization of the total operating cost and maximization of the consumer's comfort index. Then, the solution, obtained from the first stage is delivered to the distribution system operator (DSO). Then, at the second stage, the DSO determines the optimal configuration of the system with the aim of minimizing operating costs of the main grid and the penalty of deviating from microgrid scheduling. Note that this deviation is due to the difference in power exchange requested by the microgrids from the power exchange finalized by the DSO. The presented two-stage optimization problem is modeled in a mixed-integer linear programing (MILP) framework with four case

[*] Amir.mansouri24@gmail.com

studies, and solved in GAMS by using the GURUBI solver. The simulation results show that in the cases the DSO is able to reconfigure the system, the deviation from the optimal scheduling of microgrids would be considerably lower than the cases with fixed system configuration.

**Keywords:** Multi-objective optimization; Distribution feeder reconfiguration; Microgrids; Renewable energy resources, Smart homes; Consumers' comfort index.

**Nomenclature**

***Abbreviations***

| | |
|---|---|
| CV | Convenience Value |
| ENS | Energy Not Supplied |
| EEC | Estimated Energy Consumption |
| LOT | Length of Operation Time |
| PCV | Preferred Convenience Value |
| PTR | Preferred Time Range |
| UCL | User's Convenience Level |
| UTR | Utilization Time Range |

***Indices***

| | |
|---|---|
| $D_i^g$ | Set of connected gas turbines to network buses |
| $D_{mg}^i$ | Set of connected network buses belongs to microgrids |
| $D_i^{st}$ | Set of connected network buses to substation |
| $D_i^{pv}$ | Set of connected Photovoltaic panels to network buses |
| $D_i^w$ | Set of connected wind turbines to network buses |
| $D_{mg,t}^{ij-}$ | Dynamic set of connected network branches to microgrid with negative flow |
| $D_{mg,t}^{ij+}$ | Dynamic set of connected network branches to microgrid with positive flow |
| $g$ | Gas turbine index |
| $h$ | Heaviside time window index |
| $i,j$ | Network bus index |
| $mg$ | Microgrid service area index |
| $l$ | Branch index |
| $n,m$ | Appliances index |
| $pv$ | Photovoltaic panel index |
| $PTR^n$ | Preferred time range of appliances |
| $s$ | Scenario index |
| $st$ | Substation index |
| $t,tt$ | Time index |
| $UTR^n$ | Utilization time range of appliances |
| $w$ | Wind turbines index |

***Scalars***

| | |
|---|---|
| $\Delta t$ | Time step (h) |

| | |
|---|---|
| $\eta^{ch} / \eta^{dch}$ | Charging/Discharging efficiency of EES (%) |
| $\eta^{conv}$ | EES's converter efficiency (%) |
| $\eta_{pv}^{conv}$ | PV's converter efficiency (%) |
| $\eta^{gen}$ | Gas turbines efficiency (%) |
| $M$ | A positive big number |
| $N^{sw}$ | Total switching limit |

***Parameters***

| | |
|---|---|
| $\beta_n$ | Damping coefficient in preferred convenience curve |
| $EEC_n$ | Estimated energy consumption of appliances (kWh) |
| $E_w^0 / E_{pv}^0$ | Initial stored energy in EES units (kWh) |
| $E_w^{\max} / E_{pv}^{\max}$ | Maximum rate of energy stored in EES units (kWh) |
| $E_w^{\min} / E_{pv}^{\min}$ | Minimum rate of energy stored in EES units (kWh) |
| $G_{i,j}^{line} / B_{i,j}^{line}$ | Conductance/Susceptance of network branches (S) |
| $G_{std}$ | Irradiation of sun at the standard condition ($W/m^2$) |
| $LOT_n$ | Length of operation time of appliances (h) |
| $P_{i,t,s}^{fix}$ | Active fix demand in network buses (kW) |
| $\pi_t^e$ | Electricity price ($/kWh) |
| $\pi_g^{gen}$ | Gas price ($/kWh) |
| $\pi_{mg}^{penalty}$ | Penalty cost for deviating from the microgrids scheduling ($/kWh) |
| $P_g^{\min} / P_g^{\max}$ | Max/Min active power generation limit of gas turbines (kW) |
| $P_w^{ch,\max} / P_{pv}^{ch,\max}$ | Maximum charging rate of EES units (kW) |
| $P_w^{dch,\max} / P_{pv}^{dch,\max}$ | Maximum discharging rate of EES units (kW) |
| $P_{pv}^r$ | Rated active power of Photovoltaic panels (kW) |
| $P_w^r$ | Rated active power of wind turbines (kW) |
| $\pi_{pv}^{solar}$ | Solar power price ($/kWh) |
| $\pi_w^{wind}$ | Wind power price ($/kWh) |
| $Q_g^{\min} / Q_g^{\max}$ | Max/Min reactive power generation limit of gas turbines (kVar) |
| $r_{i.j} / x_{i.j}$ | Resistance/Reactance of network branches (ohm) |
| $\rho_s$ | Probability of scenario s (%) |
| $S_b / S_b^2$ | Base/Quadratic value of Piecewise block ($kVA/kVA^2$) |
| $S_{i,j}^{\max}$ | Maximum Apparent power of network branches (kVA) |
| $\theta_{i,t,s}^{\min} / \theta_{i,t,s}^{\max}$ | Max/Min voltage Angle (rad) |
| $T_{n_1,n_2}^{gap}$ | Maximum time gap between consecutive appliances (h) |
| $t_n^{start} / t_n^{end}$ | Starting/ending points of PTR for appliances (h) |
| $V_{i,t,s}^{\min} / V_{i,t,s}^{\max}$ | Max/Min voltage Magnitude (p.u.) |
| $v_i / v_r / v_o$ | Wind turbine characteristics (cut-in/rated/cut-out speed) (m/s) |
| $w_n$ | Weight coefficient of appliances |
| $\xi_{i,j}^{line}$ | Power factor of network branches |

***Variables***

| | |
|---|---|
| $\alpha_{i,j,t,s,b}$ | The piecewise block operating point |
| $C_{g,t,s}^{gen}$ | Operating cost of micro turbines ($) |
| $C_{pv,t,s}^{solar}$ | Operating cost of PV panels ($) |
| $C_{w,t,s}^{wind}$ | Operating cost of wind turbines ($) |
| $Cost_{mg,s}$ | Operation cost of microgrid ($) |
| $CV_{i,s,n}$ | User's convenience value (%) |
| $Comfort_{mg,s}$ | Users' comfort level in each microgrid (%) |
| $E_{w,t,s} / E_{pv,t,s}$ | Energy stored in EES (kWh) |
| $G_{pv,t,s}$ | Sun irradiance (W/m$^2$) |
| $\mu$ | Multi-Objective normalized value |
| $\mu^1$ | Normalized value of Operation cost |
| $\mu^2$ | Normalized value of Users' comfort level |
| $P_{pv,t,s}^{solar}$ | Active generated power by PV panel (kW) |
| $P_{w,t,s}^{wind}$ | Active generated power by wind turbines (kW) |
| $P_{i,j,t,s}^{loss}$ | Active power loss in network branches (kW) |
| $P_{i,t,s,n}^{schedule}$ | Active schedulable demand in network buses (kW) |
| $P_{g,t,s}^{gen} / Q_{g,t,s}^{gen}$ | Active/Reactive generated power by gas turbines (kW/kVar) |
| $P_{i,t,s}^{demand} / Q_{i,t,s}^{demand}$ | Active/Reactive power demand in network buses (kW/kVar) |
| $P_{st,t,s}^{sub} / Q_{st,t,s}^{sub}$ | Active/Reactive power generation of substations (kW/kVar) |
| $P_{i,t,s}^{inj} / Q_{i,t,s}^{inj}$ | Active/Reactive power injection at network buses (kW/kVar) |
| $P_{i,j,t,s}^{line} / Q_{i,j,t,s}^{line}$ | Active/Reactive power transferred in network branches (kW/kVar) |
| $P_{w,t,s}^{ch}$ | Charging active power of EES units (kW) |
| $P_{pv,t,s}^{dch}$ | Discharging active power of EES units (kW) |
| $PCV_{t,n}$ | Preferred convenience value (%) |
| $S_{i,j,t,s}^{line}$ | Apparent power transferred in network branches (kVA) |
| $\theta_{i,t,s}^{bus}$ | Angle of voltage in network buses (rad) |
| $UCL_{i,s}$ | User's convenience level (%) |
| $V_{i,t,s}^{bus}$ | Magnitude of voltage in network buses (p.u.) |
| $v_{w,t,s}$ | Wind speed (m/s) |

***Decision Variables***

| | |
|---|---|
| $I_{i,t,s,n}^{appliance}$ | Indicator for scheduling appliances |
| $I_{pv,t,s}^{ch} / I_{pv,t,s}^{dch}$ | Indicator of PV panels' EES in charging/discharging mode |
| $I_{w,t,s}^{ch} / I_{w,t,s}^{dch}$ | Indicator of wind turbine's EES in charging/discharging mode |
| $I_{l,t}^{flow}$ | Indicator for status of network branches |
| $I_{i,j,t}^{flow} / I_{j,i,t}^{flow}$ | Indicator of power flow direction in network branches |
| $I_{g,t,s}^{gen}$ | Indicator of gas turbines |
| $I_{i,t,s,n,h}^{step}$ | Indicator of time window |
| $I_{i,t,s,n}^{turn-on} / I_{i,t,s,n}^{turn-off}$ | Indicator of starting/ending points for scheduling appliances |

## 1-Introoduction

### 1-1- Background and Motivation

In the last two decades, with the restructuring of the electricity market, the penetration rate of local generation units in distribution systems has increased dramatically. Generation units consist of renewable or non-renewable energy sources and provide the load of the customers near the consumption points. In modern distribution systems, these generation units are integrated with electrical energy storage (EES) systems and managed by a central control system, which is called the microgrid [1]. It should be mentioned that the microgrid can operate in both grid-connected and islanded modes. In the grid-connected mode, microgrid is able to exchange power with the distribution system, while in islanded mode, the microgrid uses its own generation units and EES systems to meet the demand of its consumers [2].

Microgrids play an important role in transforming existing grids into smart grids. Generally, microgrids lead to reduced operating costs, reduced emissions, improved energy efficiency, and increased system reliability. It should be noted that in the problem of integrated operation of microgrids, in addition to the economic aspects, the technical and security aspects must also be considered [3]. Therefore, in this paper, a two-stage framework is presented, in the first level of which each microgrid does its day-ahead scheduling taking into account the technical and economic aspects, and then in the second stage, the final scheduling of the entire network with consideration of security aspects is done by DSO.

Recently, the focus of many studies has been on achieving a more sustainable structure for the integrated energy management of multiple microgrids. In the competitive market, the main purpose of microgrids is to meet the demand of their consumers at the lowest cost. It should be noted that the operating cost of microgrids depends on their day-ahead scheduling [4].

Uncertainties due to load, renewable energy resources (RERs) power generation and electricity prices significantly affect microgrid scheduling and pose a serious challenge for microgrid operators [5]. Therefore, it is important to consider these uncertainties in microgrid scheduling problem. In this regard, in this paper, uncertainties of load demand, electricity prices and output power of RERs are considered so that scheduling is robust against the fluctuations of generation and consumption.

The use of EES systems is one of the most effective approaches to deal with uncertainties and increase system flexibility [6]. EES systems, if installed next to RERs, store the surplus generation of these resources and then inject it into the network during peak hours. This performance not only prevents the curtailment of excess RERs power but also reduces operating cost. Besides, the shortage of generation of RERs due to unfavorable weather conditions can be compensated by the energy stored in EES systems. It should be noted that in the model proposed in this paper, an EES system is considered next to each RER.

The other two approaches to enhance operational flexibility are DFR and the demand response programs. By implementing DFR, the system operator changes the network topology in order to achieve goals such as reducing operating costs, reducing losses, and enhancing reliability. It should be mentioned that DFR is only applicable to radial networks. Noted that in the model proposed in this paper, DFR is performed by DSO with the aim of reducing the deviation of the final schedule of microgrids from their optimal schedule [7]. The participation of traditional and smart loads in demand response (DR) programs and the use of their active role in the electricity market can be an important help to improve system flexibility. On the other hand, participation in DR programs improves the load demand curve of consumers and reduces operating costs. Noted that the implementation of DR programs should be such that the comfort index of consumers always

remains at a desirable level. Hence, in this paper, the consumers' comfort index is considered as one of the objectives of the problem.

**1-2 Literature Review**

Increasing the penetration rate of RERs in distribution systems, despite reducing emissions and operating costs, has led to increased operating uncertainties [8]. Therefore, many studies have examined the problem of microgrid energy management by considering uncertainties. For instance, Ref. [9] provides a new framework for energy management of residential microgrids, in which the ten-state Markov chain is used to model the uncertainty of photovoltaic (PV) panels' generation. The proposed model is implemented on a real case study in France and the results show an improvement in performance and a 13.2% increase in microgrid profits. Ref. [10] provides a framework for microgrid energy management. In this study, rolling time horizon, adaptive neuro-fuzzy inference systems trained by clustering and neuro-fuzzy min-max classifier, Mamdani fuzzy inference system, support vector regression, echo state network and multilayer perception strategies are utilized for energy management system modeling and the results indicate that the rolling time horizon method has a more accurate performance in predicting in the presence of uncertainties. Also, in this study, a graphical interface is proposed to display the energy flow in each microgrid. In [11] a fuzzy logic-based energy management framework is presented for microgrids. The objective function of the proposed model is profit maximization of microgrid and in order to solve it, a hierarchical genetic algorithm has been utilized. The results of this study mirrored that the proposed model has improved system performance related to the profit by about 10%. Ref. [12] presents a two-stage stochastic framework for microgrid energy management, in which Apache Spark is used to improve the performance of the scalable stochastic optimization model. In this study, to deal with wind speed uncertainties, the problem is formulated based on

chance constrained method. The model is solved using both historical information and Apache Spark methods, and the results show that the use of Apache Spark has reduced production costs by 3.92% and improved system resilience.

As mentioned, DFR enhances system flexibility by rerouting power flow [13]. Therefore, in many studies, microgrid scheduling has been done considering DFR implementation. Ref. [7] provides a coordinated model for microgrid scheduling, in which DFR, DR programs, and EES systems are considered to enhance operating flexibility. In this study, an improved point estimation method (PEM) has been used to model the output power uncertainties of wind turbines and PV panels and the objective function is to minimize the operating cost of microgrid. The model is implemented on a 33-bus distribution network and the results demonstrate that the proposed model has reduced losses by 34.03%. Also, the results show that the implementation of DFR has led to a 10.83% reduction in the cost of purchasing energy. Ref. [14] has used the coordinated implementation of DFR and DR program in order to optimally exploit the distribution system. In this study, the conditional value-at-risk (CVaR) model is used to model the consumers' comfort index, which considers the risk of exceeding the comfort limit. In order to model wind speed uncertainties, Markov decision process (MDP) is utilized and the results indicate that the coordinated implementation of DFR and DR program covers wind speed prediction error. The results also illustrate that the MDP method has reduced operating costs by 2% to 7% compared to the stochastic method. Ref. [15] presents a deterministic multi-objective model based on the chaos disturbed beetle antennae search (CDBAS) optimization algorithm. The objectives of this research are loss minimization, load balance index and voltage deviation index and the proposed model has been implemented on both 69-bus and 118-bus distribution networks. Finally, the results show that the use of the CDBAS algorithm not only increases the solution speed but also reduced losses in 69-

bus and 118-bus networks by 39.42% and 10.99%, respectively. Ref. [16] introduces an energy management framework to cover phase balancing in grid interfaced photovoltaic / fuel cell system. In this regard, a phase balancing control method is provided to maintain network quality in unbalanced loading situations. The effectiveness of the proposed model has been proven by implementing on different networks.

With the advent of DR programs in the last two decades, the role of end-users in the power market has become much more prominent [17]. Meanwhile, smart homes have a greater impact on system operation than traditional homes, due to their Internet of Things (IoT)-based appliances. One of the constraints that must be considered during the implementation of DR programs is the consumers' comfort index. Hence, in recent years, many researches have done microgrid scheduling considering consumers' comfort index. In Ref. [18], the problem of smart home energy management is solved by considering a price-based DR (PBDR) program. The objectives of this model include reducing operating costs, improving consumers' comfort index and alleviating peak to average ratio (PAR), and the wind-driven bacterial foraging algorithm (WBFA) has been utilized to solve the model. The proposed algorithm automatically responds to PBDR programs to deal with the major problem of these programs, which is the limitation of consumer's knowledge in response to receiving DR signals. The simulation results show that applying DA, RTP and TOU pricing programs reduced costs by 27.6%, 40% and 52.1%, respectively. Ref. [19] presents a model for energy management of a smart home in the presence of RER, EES systems and electric vehicles. In the proposed model, the investment costs of EES systems and electric vehicles are considered and the final model is formulated as a MILP problem. The simulation results demonstrate that smart home appliance scheduling with the participation of EES and electric vehicles not only reduces the operating cost by about 29% but also improves the comfort index of

consumers. In [20], a deterministic multi-objective optimization framework for energy management of a residential microgrid is presented, in which smart home appliances scheduling is done based on IoT concept. In order to solve the model, the improved butterfly optimization algorithm is utilized and the results indicate that this algorithm leads to an increase in convergence speed. Also, the results show that the operation of the microgrid in the island mode increases the operating cost by 9% to 17%. In [21], smart home scheduling has been done using a scheduling algorithm consisting of three artificial intelligence techniques. In the proposed model, support vector regression is used to predict the power of the next day and the level of consumers' comfort index is determined by the K-means clustering algorithm. The scheduling problem is modeled as a two-objective optimization problem, the objectives of which include operating costs and consumers' comfort index. Finally, the scheduling problem is solved by the NSGA-II algorithm and the results show that the proposed model reduces the operating cost by 51.4%.

The authors in [22] present a model for the optimal operation of electricity and gas networks in the presence of smart homes, electric vehicles (EVs) and a new hybrid heating system. The proposed model is formulated in a two-objective form, the objectives of which are to minimize the cost of scheduling and minimize the discomfort index. Smart homes are considered as flexible loads and the simulation results show that the use of hybrid heating system reduces 22.8% and 21% of operating costs in electricity and gas networks, respectively. Ref. [23] presents an optimal model for energy management of a smart building equipped with PV-thermal panels. In the proposed model, a heating storage system is used for better exchange with electricity and heat networks. The case study is a real building in Western Denmark and the results show that PV-thermal panels have led to more efficient use of solar radiation energy. The authors in [24] proposed a robust optimization model for the operation of interconnected microgrids in which

several energy hubs are considered. In order to ensure the privacy of microgrids and the decentralization of the scheduling problem, the alternating direction method of multipliers (ADMM) has been utilized. The results show that doubling the system robustness rate leads to a 19% increase in operating cost. Ref. [25] presents a multi-objective model for energy management of multi-microgrids in the presence of EVs. In this study, an enhanced neural network method has been utilized to predict the charging pattern of EVs. Objective-functions include losses, operating costs and emissions, and the results indicate that using the enhanced neural network method proposed in this study reduces the forecast error by 36.86%. The authors in [26] proposed a two-objective model for the coordinated operation of electricity and gas networks in the presence of smart homes. The epsilon-constrained method is employed for two-objective modeling of the optimization problem and the objective functions are operation cost and emissions. The problem is modeled as MILP problem and the results indicate that a 2.87% reduction in emissions leads to a 0.75% increase in operating cost. In addition, the results show that a 21.93% increase in the comfort index increases the operating cost by 41%. An energy management framework for day-ahead scheduling of interconnected microgrids considering DR program is presented in [27]. In this study, microgrids use a novel deep-learning artificial neural network (ANN) model to predict load demand and generation of RERs, and the results demonstrate that the coordinated performance of EES systems and DR program has led to a reduction in operating costs.

**1-3- Research Gap**

Table 1 provides a comparison between the model proposed in this paper and recent studies. A review of recent researches shows that most studies have solved the DFR problem with the aim of reducing losses, voltage stability and enhancing reliability, and none of the studies has solved the DFR problem in the presence of smart homes and considering the comfort index of customers.

Therefore, in this paper, a comprehensive model is presented in which microgrids include traditional and smart homes and the DFR problem is solved according to the operation cost and the comfort index of the customers.

**1-4- Contribution**

This paper presents a two-stage framework for the scheduling of microgrids and DFR. The model has been implemented on the modified IEEE 118-bus test system, including ten microgrids with traditional loads and smart homes. Besides, the uncertainties due to the load demand, market price, and renewable power generation have been applied to the model to take into consideration realistic conditions. The problem has been formulated as a two-stage optimization problem to efficiently address the large-scale optimization problem with a high number of continuous and discrete variables. The first stage solves the day-ahead scheduling of microgrids as a two-objective optimization problem, using the min-max fuzzy method. The objectives are defined as the minimization of the total operating cost minimization and the maximization of consumers' comfort index. The second stage is devoted to the optimal DFR, carried out by the DSO, aimed at minimizing the deviation from the optimal scheduling of microgrids, determined at the first stage. The novelties of the paper can be briefly stated as follows:

- Proposing a two-stage optimization framework for scheduling of microgrids and DFR
- Considering smart homes and traditional loads in the model
- Solving the day-ahead scheduling problem of microgrids in the form of a two-objective problem considering operation cost and consumers' comfort index
- Solving the DFR problem with regard to the optimal scheduling of microgrids
- Investigating the impact of different objective functions on smart homes' scheduling

This paper organizes as follows. The system description is presented in Section 2. The mathematical problem formulation including the objective functions and corresponding constraints are addressed in Section 3. The algorithms and flowchart for solving the proposed model are presented in Section 4. Simulation results and the comprehensive discussion are addressed in Section 5 of this paper. The concluding remarks are presented in the last section of this paper.

Table 1. Comparison of this study with recent researches.

| Refs. | Objectives | Mathematical Model | Problem Modeling | | Multi-Stage | DFR | Home Appliances | | Comfort Index | DR | EES | RER | | Uncertainty |
|---|---|---|---|---|---|---|---|---|---|---|---|---|---|---|
| | | | Single-Objective | Multi-Objective | | | IoT | Fix | | | | Wind | PV | |
| [10] | Profit | MILP | ✓ | × | × | ✓ | × | ✓ | × | × | ✓ | × | ✓ | ✓ |
| [7] | Cost<br>Profit | MINLP | ✓ | × | × | ✓ | × | ✓ | × | ✓ | × | ✓ | ✓ | ✓ |
| [14] | Cost | MINLP | ✓ | × | × | ✓ | × | ✓ | ✓ | ✓ | ✓ | ✓ | × | ✓ |
| [28] | Power Loss<br>Voltage Deviation | MILP | × | ✓ | × | ✓ | × | ✓ | × | ✓ | ✓ | × | ✓ | × |
| [29] | Operation Cost<br>Interruption Cost<br>Switching Cost | MILP | ✓ | × | × | ✓ | × | ✓ | × | × | ✓ | × | × | × |
| [30] | ENS<br>Power Loss | MINLP | × | ✓ | × | ✓ | × | ✓ | × | × | × | × | × | × |
| [21] | Cost<br>Comfort Index | MINLP | × | ✓ | × | × | ✓ | × | ✓ | × | ✓ | ✓ | ✓ | × |
| [19] | Cost | MILP | ✓ | × | × | × | ✓ | × | ✓ | × | ✓ | × | ✓ | ✓ |
| [20] | Cost | MILP | ✓ | × | × | × | ✓ | × | × | × | ✓ | ✓ | ✓ | × |
| [18] | Cost<br>PAR<br>Comfort Index | MINLP | ✓ | × | × | × | ✓ | × | ✓ | ✓ | ✓ | × | ✓ | × |
| [31] | Cost | MILP | ✓ | × | × | × | ✓ | × | ✓ | × | ✓ | × | ✓ | ✓ |
| [32] | Cost | MILP | ✓ | × | × | × | ✓ | × | × | × | ✓ | × | ✓ | × |
| [33] | Power Unbalance | MINLP | ✓ | × | × | × | × | ✓ | × | × | ✓ | ✓ | × | × |
| [34] | Cost<br>Comfort Index | MILP | × | ✓ | ✓ | × | ✓ | × | ✓ | ✓ | ✓ | ✓ | ✓ | × |
| [11] | Profit<br>Fuzzy Rules | MILP | × | ✓ | × | × | × | ✓ | × | × | ✓ | × | ✓ | ✓ |
| [12] | Cost | MILP | ✓ | × | ✓ | × | × | ✓ | × | × | ✓ | ✓ | ✓ | ✓ |
| [9] | Forecast Error | MINLP | ✓ | × | × | × | × | × | × | × | ✓ | × | ✓ | ✓ |
| [35] | Cost | MILP | ✓ | × | × | × | × | × | ✓ | × | ✓ | ✓ | ✓ | ✓ |
| [36] | Cost<br>Comfort Index | MINLP | × | ✓ | × | × | ✓ | × | ✓ | ✓ | ✓ | ✓ | ✓ | ✓ |
| [22] | Cost<br>Thermal Comfort | MILP | ✓ | × | × | × | ✓ | × | ✓ | × | ✓ | × | ✓ | ✓ |
| [23] | Cost | MINLP | ✓ | × | × | × | × | ✓ | × | × | × | × | ✓ | × |

| | | | | | | | | | | | | | | |
|---|---|---|---|---|---|---|---|---|---|---|---|---|---|---|
| [24] | Cost | MIQCP | ✓ | × | ✓ | × | × | ✓ | × | × | ✓ | ✓ | ✓ | ✓ |
| [25] | Power Loss<br>Cost<br>Emission | MINLP | × | ✓ | × | × | × | ✓ | × | × | ✓ | ✓ | ✓ | ✓ |
| This Paper | Cost<br>Comfort Index | MILP | × | ✓ | ✓ | ✓ | ✓ | ✓ | ✓ | ✓ | ✓ | ✓ | ✓ | ✓ |

## 2- System description

The test system, used in this paper to assess the proposed model is the modified IEEE 118-bus system, comprising ten microgrids, depicted in Fig. 1. As this figure indicates, each microgrid supplies its load demand by utilizing RESs, including wind and solar power generation, non-renewable sources, including a gas-turbine, and also by transacting power with the upstream network. It is noteworthy that an electrical energy storage (EES) system has been used along with the renewable energy technologies. Moreover, 15 switches have been considered for the DFR, as depicted in Fig. 1 in red. Each microgrid serves both traditional load demand and smart homes, and the day-ahead scheduling is done, aimed at maximizing the smart homes' comfort index. The locations of smart homes in the microgrids are specified in green. The controllable loads of a smart home comprise a washing machine, a clothes dryer, a dishwasher, an iron, a microwave oven, a cooker, an electric kettle, and a toaster. In addition, fixed loads of each smart home relate to the cooling, heating, and lighting system. Every smart home is equipped with self-generation technologies, including a PV panel and an EES system to mitigate the amount of the bill and increase the system flexibility.

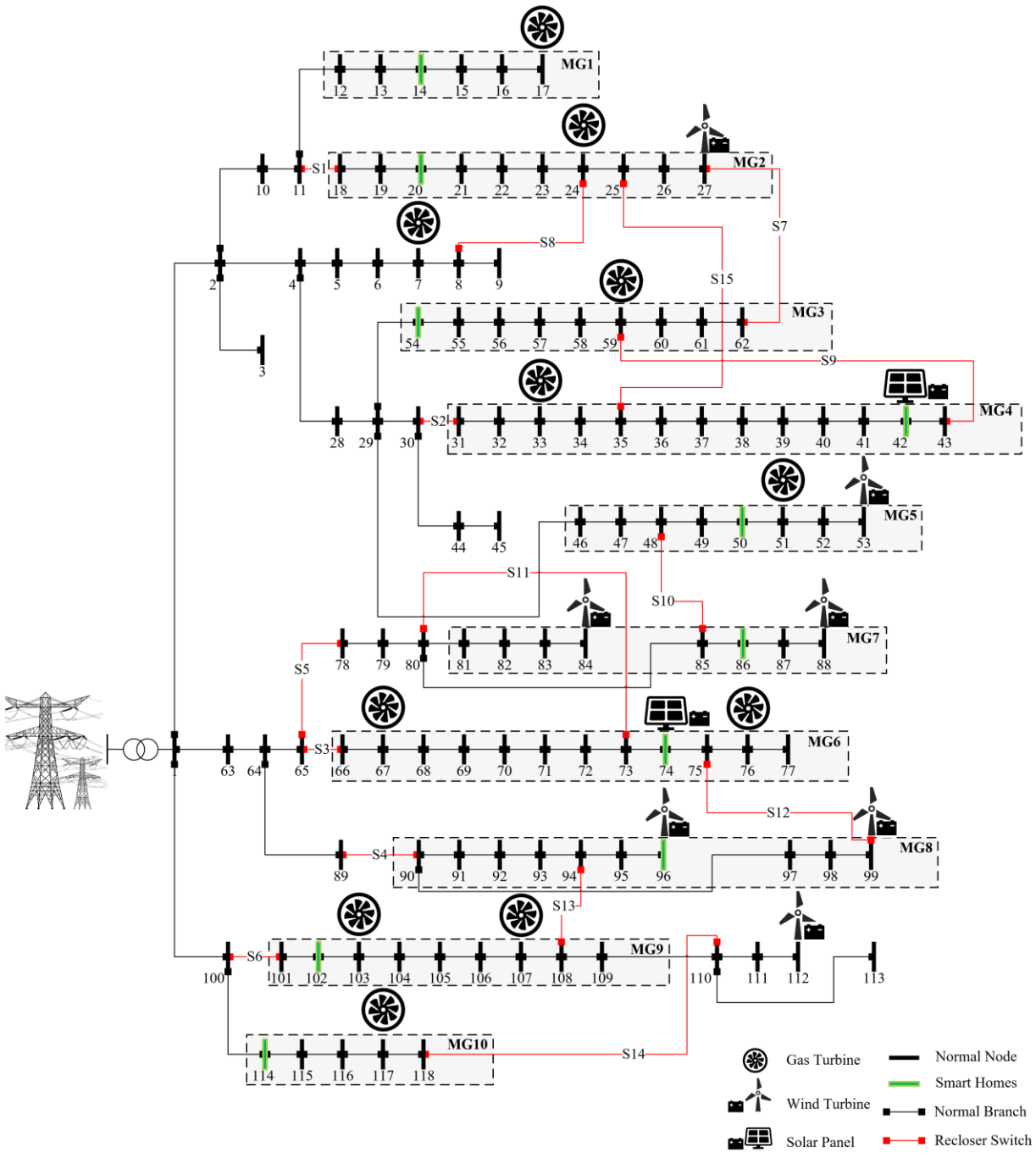


Fig. 1. The overview of the modified IEEE 118-bus distribution system.

## 3- Formulation

This section presents the mathematical formulation of the problem.

- **Objective Functions**

The objective functions of the first stage of the problem are defined as the minimization of the total operating cost and maximization of the consumers' comfort index, expressed in (1a) and (1b) respectively, in the service area of each microgrid. It should be noted that the resulting multi-objective problem is solved by employing the min-max fuzzy method [37]. In this regard, expression (1c) indicates the membership function, assigned to each objective.

The objective function of the second stage is presented in Eq. (1d), which is to minimize operating costs of the main grid and the penalty of deviating from microgrids scheduling. The objective function indicates that the network will be penalized if fails to satisfy the requested power exchange of the microgrids. $P^{line}_{i,j,t,s}$ is the requested power exchange by the microgrid, while $P^{line}_{i,j,t,s}$ is the power exchange finalized by the DSO. $\pi^{penalty}_{mg}$ represents the penalty cost. It is noteworthy that the objective function of this stage is solved from the DSO point of view.

$$\min \sum_{s=1}^{S} \rho_s \sum_{mg=1}^{MG} Cost_{mg,s} \tag{1a}$$

$$\max \sum_{s=1}^{S} \rho_s \sum_{mg=1}^{MG} Comfort_{mg,s} \tag{1b}$$

$$\max \mu \leq \begin{cases} \mu^1 = \dfrac{Cost^{\max} - Cost^{opt}}{Cost^{\max} - Cost^{\min}} \\ \mu^2 = \dfrac{Comfort^{opt} - Comfort^{\min}}{Comfort^{\max} - Comfort^{\min}} \end{cases} \tag{1c}$$

$$\min \sum_{s=1}^{S} \rho_s \left[ \begin{array}{l} \sum_{t=1}^{T} \sum_{i \in D^{i}_{mg}}^{I} \left( \sum_{g \in D^{g}_{i}}^{G} C^{gen}_{g,t,s} + \sum_{w \in D^{w}_{i}}^{W} C^{wind}_{w,t,s} + \sum_{pv \in D^{pv}_{i}}^{pv} C^{solar}_{pv,t,s} \right) + \sum_{t=1}^{T} \sum_{st \in D^{st}_{i}}^{ST} \pi^{e}_{t} P^{sub}_{st,t,s} \Delta t \\ \sum_{mg=1}^{MG} \pi^{penalty}_{mg} \sum_{t=1}^{T} \sum_{(i,j) \in \left( D^{ij+}_{mg,t}, D^{ij-}_{mg,t} \right)}^{I,J} \left| P^{line}_{i,j,t,s} - P^{line}_{i,j,t,s} \right| \Delta t \end{array} \right] \tag{1d}$$

- **Power Flow**

The linearized AC power flow (ACPF) relationships, used in this paper are represented in (2a)-(2o) [38]. The conductance and susceptance of the feeder are calculated as (2a) and (2b) respectively. Eqs. (2c) and (2d) represent the active and reactive power flow of lines, as functions

of voltage magnitude and angle. The active and reaction power injection of each bus to the connected branches are determined by using Eqs. (2e) and (2f), respectively. Eq. (2g) shows the apparent power flow of each line as a function of the active and reactive power flows and the average power factor of the sending and receiving buses. Inequality (2h) applies the security constraint, relating to the minimum and maximum power flow of lines. The nodal active and reactive power balance equations are stated in (2i) and (2j) respectively, and constraints (2k) and (2l) limit the voltage magnitude and voltage angle within the permitted range respectively. The system's power losses are also calculated by using relationships (2m)-(2o). In this respect, Eq. (2m) shows that power flow of each line would be specified with respect to the operating point of that line. Constraint (2n) indicates the operating point limitation of each line. Finally, Eq. (2o) gives the power losses of each line.

$$G_{i,i}^{line} = \frac{r_{i.j}}{r_{i,j}^2 + x_{i,j}^2} \tag{2a}$$

$$B_{i,i}^{line} = \frac{x_{i.j}}{r_{i,j}^2 + x_{i,j}^2} \tag{2b}$$

$$\begin{aligned} G_{i,j}^{line}\left(V_{i,t,s}^{bus} - V_{j,t,s}^{bus}\right) + B_{i,j}^{line}\left(\theta_{i,t,s}^{bus} - \theta_{j,t,s}^{bus}\right) + \frac{P_{i,j,t,s}^{loss}}{2} - M\left(1 - I_{l,t,s}^{flow}\right) \\ \le P_{i,j,t,s}^{line} \le \\ G_{i,j}^{line}\left(V_{i,t,s}^{bus} - V_{j,t,s}^{bus}\right) + B_{i,j}^{line}\left(\theta_{i,t,s}^{bus} - \theta_{j,t,s}^{bus}\right) + \frac{P_{i,j,t,s}^{loss}}{2} + M\left(1 - I_{l,t,s}^{flow}\right) \end{aligned} \tag{2c}$$

$$\begin{aligned} B_{i,j}^{line}\left(V_{i,t,s}^{bus} - V_{j,t,s}^{bus}\right) - G_{i,j}^{line}\left(\theta_{i,t,s}^{bus} - \theta_{j,t,s}^{bus}\right) - M - I_{l,t,s}^{flow} \\ \le Q_{i,j,t,s}^{line} \le \\ B_{i,j}^{line}\left(V_{i,t,s}^{bus} - V_{j,t,s}^{bus}\right) - G_{i,j}^{line}\left(\theta_{i,t,s}^{bus} - \theta_{j,t,s}^{bus}\right) + M\left(1 - I_{l,t,s}^{flow}\right) \end{aligned} \tag{2d}$$

$$P_{i,t,s}^{inj} = \sum_{j(j\neq i)}^{J} P_{i,j,t,s}^{line} \tag{2e}$$

$$Q_{i,t,s}^{inj} = \sum_{j(j\neq i)}^{J} Q_{i,j,t,s}^{line} \tag{2f}$$

$$S_{i,j,t,s}^{line} = P_{i,j,t,s}^{line} + \xi_{i,j}^{line} Q_{i,j,t,s}^{line} \tag{2g}$$

$$-S_{i,j}^{\max} I_{l,t,s}^{flow} \le S_{i,j,t,s}^{line} \le S_{i,j}^{\max} I_{l,t,s}^{flow} \tag{2h}$$

$$\sum_{st\in D_i^{st}}^{ST} P_{st,t,s}^{sub} + \sum_{g\in D_i^{g}}^{G} P_{g,t,s}^{gen} + \sum_{w\in D_i^{w}}^{W} \left(P_{w,t,s}^{wind} + P_{w,t,s}^{dch} - P_{w,t,s}^{ch}\right) + \sum_{pv\in D_i^{pv}}^{pv} \left(P_{pv,t,s}^{solar} + P_{pv,t,s}^{dch} - P_{pv,t,s}^{ch}\right) = P_{i,t,s}^{inj} + P_{i,t,s}^{Demand} \quad (2i)$$

$$\sum_{st\in D_i^{st}}^{ST} Q_{st,t,s}^{sub} + \sum_{g\in D_i^{g}}^{G} Q_{g,t,s}^{gen} = Q_{i,t,s}^{inj} + Q_{i,t,s}^{Demand} \quad (2j)$$

$$V_{i,t,s}^{\min} \le V_{i,t,s} \le V_{i,t,s}^{\max} \quad (2k)$$

$$\theta_{i,t,s}^{\min} \le \theta_{i,t,s} \le \theta_{i,t,s}^{\max} \quad (2l)$$

$$\left|S_{i,j,t,s}^{line}\right| = \sum_{b} \alpha_{i,j,t,s,b} S_b \quad (2m)$$

$$0 \le \sum_{b=1}^{B} \alpha_{i,j,t,s,b} \le 1 \quad (2n)$$

$$P_{i,j,t,s}^{loss} = r_{i,j} \sum_{b} \alpha_{i,j,t,s,b} S_b^2 \quad (2o)$$

- **DFR**

Constraints (3a)-(3c) guarantee the radiality of the network during DFR. Constraint (3a) determines the direction of power flow in the active lines (present in operation). $I_{l(i,j),t}^{flow}$ is a binary variable that determines the presence/absence of each line at time *t*. Constraint (3b) states that each bus can receive power from only one line. Constraint (3c) prevents the injection of power into the slack bus. Finally, constraint (34) limits the number of switches during operation horizon [39].

$$I_{i,j,t,s}^{flow} + I_{j,i,t,s}^{flow} = I_{l(i,j),t,s}^{flow} \quad (3a)$$

$$\sum_{j(j\neq i)}^{J} I_{j,i,t,s}^{flow} = 1 \quad (3b)$$

$$\sum_{j(j\neq i)}^{J} I_{j,i\in D_i^{st},t,s}^{flow} = 0 \quad (3c)$$

$$\sum_{t=1}^{T}\sum_{l=1}^{L} \left|I_{l,t,s}^{flow} - I_{l,t-1,s}^{flow}\right| \le N^{sw} \quad (3d)$$

- **Appliances**

As mentioned above, each microgrid includes a number of smart homes and it operates considering traditional loads and smart homes. In this respect, Eqs. (4a)-(4p) represent the relationships, required to model the operation of home appliances [40]. The load demand of each home includes two load categories as fixed and schedulable loads, shown in (4a). The hourly consumption of each

appliance is stated in (4b), while (4c) shows that the operation time of each appliance must be equal to the corresponding length of operation time (LOT). Besides, constraint (4d) states that each appliance should be activated only in its utilization time range (UTR) interval. Constraint (4e) indicates that the appliance operation is uninterruptable. It should be noted that some appliances have dependent operation. For example, first, the WM should work and after that the SD starts working. The operation of such appliances has been modeled by relationships (4f)-(4h). Constraint (4f) ensures the proper operation of each appliance. Constraint (4g) models the limitation of binary variable $H_{i,t,s,n,h}$. As constraint (4h) states, each dependent appliance should be turned on after the operation of the independent appliance is finished. Constraints (4i)-(4k) are proposed to ensure the permitted time intervals, required between the operations of dependent appliances. The consumer's comfort index is calculated in Eq. (4l) as a function of the comfort index and value factor of each appliance. Eqs. (4m) and (4n) are used to determine the user's convenience level (UCL) of the appliances and comfort level of all smart homes is calculated as (4o). As can be seen, in Eq. (4n), two exponential functions are used to determine UCL. This equation states that if the appliance activation time is in the consumers' preferred range, the UCL value will be equal to 1, and if the appliance activation time is outside the consumers' preferred range, the UCL value will decrease with a certain slope. Where, $\beta_n$ denotes damping coefficient of preferred convenience curve.

$$P_{i,t,s}^{demand} = P_{i,t,s}^{fix} + \sum_{n=1}^{N} P_{i,t,s,n}^{schedule} \tag{4a}$$

$$P_{i,t,s,n}^{schedule} = \frac{EEC_n I_{i,t,s,n}}{LOT_n} \tag{4b}$$

$$\sum_{t \in UTR^n}^{T} I_{i,t,s,n}^{appliance} = LOT_n \tag{4c}$$

$$\sum_{t \notin UTR^n}^{T} I_{i,t,s,n}^{appliance} = 0 \tag{4d}$$

$$\sum_{t \in UTR^n}^{T} \left| I_{i,t,s,n}^{appliance} - I_{i,t-1,s,n}^{appliance} \right| \leq 2 \tag{4e}$$

$$\sum_{tt\in UTR^n}^{t} I_{i,t,s,n}^{appliance} - LOT_n = \sum_h I_{i,t,s,n,h}^{step}\delta_h \quad (4f)$$

$$\sum_h^H I_{i,t,s,n,h}^{step} = 1 \quad (4g)$$

$$I_{i,t,s,m}^{appliance} \le I_{i,t,s,n,h=H}^{step} \quad (4h)$$

$$I_{i,t,s,n}^{turn-on} - I_{i,t,s,n}^{turn-off} = I_{i,t,s,n} - I_{i,t-1,s,n} \quad (4i)$$

$$0 \le I_{i,t,s,n}^{turn-on} + I_{i,t,s,n}^{turn-off} \le 1 \quad (4j)$$

$$I_{i,t,s,m}^{turn-on} - I_{i,t,s,n}^{turn-off} \le T_{n,m}^{gap} \quad (4k)$$

$$UCL_{i,s} = \frac{\sum_{n=1}^{N} w_n CV_{i,s,n}}{\sum_{n=1}^{N} w_n LOT_n} \quad (4l)$$

$$CV_{i,s,n} = \sum_{t=1}^{T} I_{i,t,s,m}^{appliance} PCV_{t,n} \quad (4m)$$

$$PCV_{t,n} = \begin{cases} 1 & ,t \in PTR \\ \beta_n e^{t-t_n^{start}} & ,t < t_n^{start} \\ \beta_n e^{t_n^{end}-t} & ,t > t_n^{end} \end{cases} \quad (4n)$$

$$Comfort_{mg,s} = \sum_{i\in D_{mg}^{i}}^{I} UCL_{i,s} \quad (4o)$$

- **Generation Units**

Relationships (5a)-(5h) relate to the power generation by DERs and their associated operating cost. In this regard, Eq. (5a) shows the hourly power generation equation of the wind turbine, which is a function of the hourly wind speed and turbine characteristics [41]. The power, generated by the PV panel is in accordance with Eq. (5b) as a function of the hourly solar [34]. Noted that the converter efficiency ( $\eta_{pv}^{conv}$ ) is considered to be 95%. As Eq. (5c) shows, the power, generated by the MT is a function of the input gas and turbine efficiency. The constraints of active and reactive power generation of the MT are represented in (5d) and (5e) respectively. The operating costs of the MTs, wind turbines, and PV panels are stated in Eqs. (5f)-(5h) respectively. The total operating cost of each microgrid is also calculated as Eq. (5i).

$$P_{w,t,s}^{wind}=\begin{cases}0, & v_{w,t,s}<v_i, v_{w,t,s}>v_o\\ P_w^r\dfrac{v_{w,t,s}-v_i}{v_r-v_i}, & v_i\le v_{w,t,s}<v_r\\ P_w^r, & v_r\le v_{w,t,s}<v_o\end{cases} \tag{5a}$$

$$P_{pv,t,s}^{solar}=\frac{G_{pv,t,s}}{G_{std}}P_{pv}^r\eta_{pv}^{conv} \tag{5b}$$

$$P_{g,t,s}^{gen}=G_{g,t,s}^{gen}\eta^{gen} \tag{5c}$$

$$P_g^{\min}I_{g,t,s}^{gen}\le P_{g,t,s}^{gen}\le P_g^{\max}I_{g,t,s}^{gen} \tag{5d}$$

$$Q_g^{\min}I_{g,t,s}^{gen}\le Q_{g,t,s}^{gen}\le Q_g^{\max}I_{g,t,s}^{gen} \tag{5e}$$

$$C_{g,t,s}^{gen}=\pi_g^{gen}P_{g,t,s}^{gen}\Delta t \tag{5f}$$

$$C_{w,t,s}^{wind}=\pi_w^{wind}P_{w,t,s}^{wind}\Delta t \tag{5g}$$

$$C_{pv,t,s}^{solar}=\pi_{pv}^{solar}P_{pv,t,s}^{solar}\Delta t \tag{5h}$$

$$\begin{aligned}Cost_{mg,s}=&\sum_{t=1}^{T}\sum_{i\in D_{mg}^i}^{I}\left(\sum_{g\in D_i^g}^{G}C_{g,t,s}^{gen}+\sum_{w\in D_i^w}^{W}C_{w,t,s}^{wind}+\sum_{pv\in D_i^{pv}}^{pv}C_{pv,t,s}^{solar}\right)\\&+\sum_{t=1}^{T}\left[\pi_t^e\left(\sum_{(i,j)\in D_{mg,t}^{ij+}}^{I,J}P_{i,j,t,s}^{line}-\sum_{(i,j)\in D_{mg,t}^{ij-}}^{I,J}P_{i,j,t,s}^{line}\right)\Delta t\right]\end{aligned} \tag{5i}$$

- **Network' EES system**

The renewable power generation units are all equipped with an EES system. In this respect, relationships (6a)-(6h) show the operation model of the EES systems, installed along with the wind turbines. Eq. (6a) indicates that the energy, available in the EES system at each hour is a function of the energy, stored in the system in the previous hour and the charging/discharging power at the present hour. It should be noted that $\Delta t$ is time step and its value is equal to 1 hour. Constraint (6b) shows the initial amount of energy, stored in the EES system at the beginning of the scheduling period. The limitations on the energy, stored in the system has also been stated in (6c), while constraints (6d) and (6e) force the charging and discharging rates to be within the permitted range respectively. As constraint (6f) shows, the EES system is obliged to operate in either charging or discharging mode. Furthermore, according to constraint (6g), the amount of energy that must be available in the EES system at the end of the scheduling period should be equal or greater than the initial amount [42].

$$E_{w,t,s} = E_{w,t-1,s} + \left( P_{w,t,s}^{ch} \eta^{ch} - \frac{P_{w,t,s}^{dch}}{\eta^{dch}} \right) \Delta t \quad (6a)$$

$$E_{w,t=0,s} = E_w^0 \quad (6b)$$

$$E_w^{\min} \le E_{w,t,sc} \le E_w^{\max} \quad (6c)$$

$$0 \le P_{w,t,s}^{ch} \le P_w^{ch,\max} I_{w,t,s}^{ch} \quad (6d)$$

$$0 \le P_{w,t,s}^{dch} \le P_w^{dch,\max} I_{w,t,s}^{dch} \quad (6e)$$

$$0 \le I_{w,t,s}^{ch} + I_{w,t,s}^{dch} \le 1 \quad (6f)$$

$$E_{w,t=24,s} \ge E_w^0 \quad (6g)$$

- **Smart home' EES system**

Relationships (7a)-(7i) indicate the operation model of the EES systems, installed next to PV panels [43]. Constraint (7a) states the limitation of the amount of energy, stored in the EES system. Constraints (7b) and (7c) show the calculation of the charging power and discharging power respectively, which are the function of the respective efficiencies and the energy, available in the EES system. The charging power and discharging power are limited as shown in (7d) and (7e) respectively. The conflict between the charging and discharging modes is avoided by using constraint (7f). The energy, stored in the EES system at each hour is determined by utilizing relationship (7g). The constraints of the initial and final values of the energy, stored in the EES system are in accordance with (7h). Condition (7i) states that the energy level of EES systems located in smart homes must be equal to or greater than the initial energy level at the last hour of scheduling.

$$E_{pv}^{\min} \le E_{pv,t,s} \le E_{pv}^{\max} \quad (7a)$$

$$P_{pv,t,s}^{ch} \Delta t \le E_{pv}^{max} \frac{(1 - E_{pv,t-1,s})}{(1-\eta^{ch})\eta^{conv}} \quad (7b)$$

$$P_{pv,t,s}^{dch} \Delta t \le E_{pv}^{max} (E_{pv,t-1,s} - 1)(1-\eta^{dch})\eta^{conv} \quad (7c)$$

$$P_{pv,t,s}^{ch} \Delta t \le \frac{E^{ch,conv}}{\eta^{conv}} I_{pv,t,s}^{ch} \quad (7d)$$

$$P_{pv,t,s}^{dch} \Delta t \le \frac{E^{dch,conv}}{\eta^{conv}} I_{pv,t,s}^{dch} \quad (7e)$$

$$0 \le I_{pv,t,s}^{ch} + I_{pv,t,s}^{dch} \le 1 \quad (7f)$$

$$E_{pv,t,s} = E_{pv,t-1,s} - \frac{\Delta t}{E_{pv}^{\max}}\left[\frac{P_{pv,t,s}^{dch}}{(1-\eta^{dch})\eta^{dch,conv}} + P_{pv,t,s}^{ch}(1-\eta^{ch})\eta^{ch,conv}\right] \quad (7g)$$

$$E_{pv,t=0,s} = E_{pv}^{0} \quad (7h)$$

$$E_{pv,t=24,s} \geq E_{pv}^{0} \quad (7i)$$

- **Uncertainty modeling process**

The uncertainties due to the load demand, market price, and renewable power generation have been applied to the problem to obtain a more realistic solution. In this regard, first, 1000 scenarios are generated for each uncertain parameter by the probability distribution functions (PDFs), using the Gaussian PDF for the load demand, market price and solar irradiance, and the Weibull PDF for the wind speed. Gaussian PDF is presented in Eq. (8a). $\mu_x$ and $\sigma_x$ denote the mean and standard deviation, respectively; $\Delta x_t$ denotes the error of the load prediction. The values of parameters $\mu_x$ and $\sigma_x$ are considered 0 and 0.3, respectively. Weibull PDF is presented in Eq. (8b). $\lambda$ and $k$ denote the scale and shape parameters, respectively [44]. The values of parameters $\lambda$ and $k$ are considered 1 and 1.5, respectively.

$$f\left(\Delta x_t;\mu_x,\sigma_x^2\right) = \frac{1}{\sqrt{2\pi\sigma_x^2}}\exp\left[-\frac{\left(\Delta x_t-\mu_x\right)^2}{2\sigma_x^2}\right] \quad (8a)$$

$$f(x;\lambda,k) = \begin{cases} \frac{k}{\lambda}\left(\frac{x}{\lambda}\right)^{k-1} e^{-\left(\frac{x}{\lambda}\right)^k} & , x \geq 0 \\ 0 & , x < 0 \end{cases} \quad (8b)$$

Afterward, the number of scenarios is reduced by employing the SCENRED2 in GAMS [45], to alleviate the computational load of the problem. It should be noted that SCENRED2 is a fundamental update of the well-known scenario reduction software SCENRED. SCENRED is a tool for reducing the number of scenarios that performs the scenario reduction process by one of the fast backward, mix of fast backward/forward and mix of fast backward/backward algorithms.

- **Multi-scenario modelling**

In this subsection, the process of multi-scenario modeling is shown [46]. To this end, each continuous PDF is discretized in order to form a set of finite states. It should be mentioned that an occurrence probability is assigned to each state. discrete sets related to different parameters forecasting errors are shown in (9a)-(9d).denotes $\rho_D^i$ th state, $i$ denotes the error related to the $e_D^i$ the probability of *i*th state, and *n* denotes the number of states of the discrete set. Discrete sets of other uncertain parameters are determined in the same way. Note that the probabilities of states are subject to constraint (9e)**.**

$$\delta_D = \left\{\left(e_D^1, \rho_D^1\right), \left(e_D^2, \rho_D^2\right), \ldots, \left(e_D^n, \rho_D^n\right)\right\} \tag{9a}$$

$$\delta_P = \left\{\left(e_P^1, \rho_P^1\right), \left(e_P^2, \rho_P^2\right), \ldots, \left(e_P^k, \rho_P^k\right)\right\} \tag{9b}$$

$$\delta_W = \left\{\left(e_W^1, \rho_W^1\right), \left(e_W^2, \rho_W^2\right), \ldots, \left(e_W^m, \rho_W^m\right)\right\} \tag{9c}$$

$$\delta_{PV} = \left\{\left(e_{PV}^1, \rho_{PV}^1\right), \left(e_{PV}^2, \rho_{PV}^2\right), \ldots, \left(e_{PV}^q, \rho_{PV}^q\right)\right\} \tag{9d}$$

$$\sum_{i=1}^{n} \rho_D^i = \sum_{i=1}^{k} \rho_P^i = \sum_{i=1}^{m} \rho_W^i = \sum_{i=1}^{q} \rho_{PV}^i = 1 \tag{9e}$$

The discrete sets obtained from Eqs. (9a) - (9d) are used to form a set of scenarios that indicate the possible deviations from the load, price, wind, and irradiance forecasted values. Each scenario has a probability ( $\rho_s^i$ ), which is equal to the product of the probabilities of the states related to that scenario, as illustrated in Eq. (9f). Also, according to Eq. (9g) the total number of obtained scenarios is equal to the product of the number of states in each discrete set.

$$\sum_{i=1}^{S} \rho_s^i = \sum_{i=1}^{S} \rho_D^i \rho_P^i \rho_W^i \rho_{PV}^i = 1 \tag{9f}$$

$$S = n \times m \times q \times k \tag{9g}$$

## 4- Methodology

Fig. 2 depicts the flowchart of the proposed model. As can be observed, the scenarios are generated by PDFs and then, they are reduced by using the SCENRED2 in GAMS. After that, at the first stage, the operation problem would be solved from the viewpoint of each microgrid, aimed at optimizing the operating cost and consumers' comfort index. It should be noted that the problem of microgrid scheduling can be solved as a single-objective or two-objective problem. In the case of choosing two-objective scheduling, a pay-off table will be formed to solve the two-objective problem of microgrids scheduling. The payoff table in multi-objective programming provides the individual optimal of the objective functions (in the diagonal). The goal of forming a payoff table is to help formulate the constraint model in the next task (membership functions), by determining the lower and upper bounds for the objective functions. A membership function is a curve that defines how each point in the input space is mapped to a membership value (or degree of membership) between 0 and 1. At the end of the first stage, the results, relating to the microgrids operation, including the new load demand curve, besides the hourly power transaction, are fixed at their optimal values and delivered to the DSO. At second stage, the DSO would be able to evaluate the possibility of the obtained scheduling of microgrids. It is also noted that the system topology can be either fixed or reconfigured at this stage. If the system is reconfigured, it is carried out, aimed at minimizing the deviation from the optimal scheduling of microgrids, determined at the first stage. If the hourly scheduling of any microgrid is not possible to implement, corrective signals (optimality cuts) would be generated by the DSO and sent to the respective microgrid. These signals are added to the problem as new constraints and the scheduling continues until satisfying the stopping criterion. In general, the presented algorithm can be interpreted as follows:

- **Step 1:** Solve microgrids day-ahead scheduling in the form of:

$$MO\begin{cases}\min OF_1 = \sum_{mg=1}^{MG} Cost_{mg} \\ \max OF_2 = \sum_{mg=1}^{MG} Comfort_{mg}\end{cases}$$

*s.t.*
(2a)-(2o), (4a)-(4o), (5a)-(5i), (6a)-(6g), (7a)-(7i)

- **Step 2:** Send microgrids' day-ahead scheduling to the DSO and convert the distribution system to the multi-zone area network.

- **Step 3:** Evaluation operation results of microgrids by DSO with/without implementing DFR in the form of:
  Min Eq. (1d)
  *s.t.*
  (2a)-(2o), (3a)-(3d), (4a)-(4o), (5a)-(5i), (6a)-(6g), (7a)-(7i)

- **Step 4:** Check power transaction violations of each microgrid:
  **For** each line, **do**:
  **If** positive error happens, **then**:
  Define lower limit for the line.
  Active positive error flag
  **If** negative error happens,
  **Then**: define upper limit for the line.
  Active negative error flag
  **Else:** Stop and return results.

- **Step 5: For** each positive error, **Do**:
  Add a cut to limit the lower level of line.
  **For** each negative error, **do**:
  Add a cut to limit the upper level of line.

- **Step 6:** Define cuts as new constraints for the scheduling problem in each iteration.
- **Step 7: Go to** step 1.

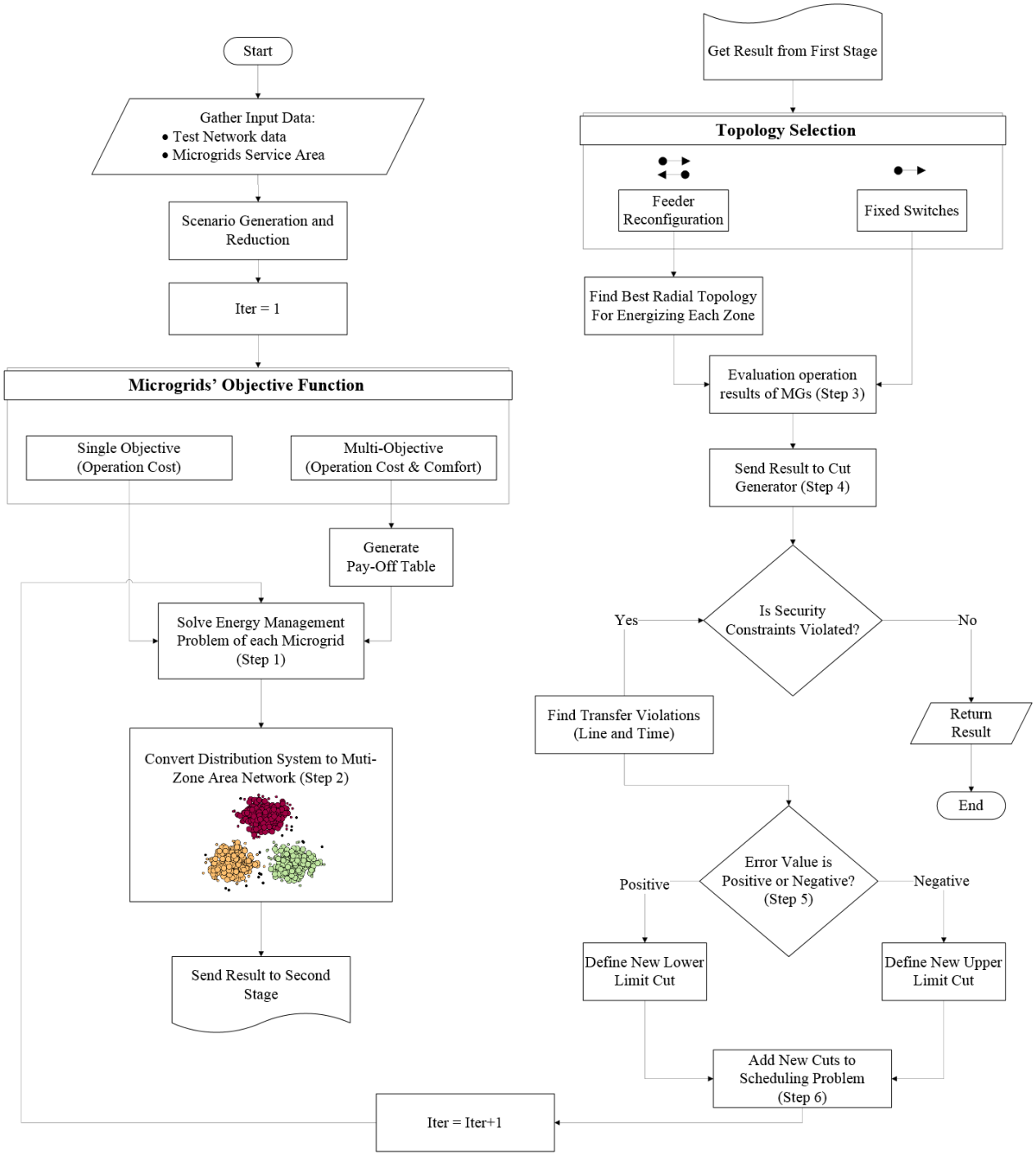


Fig. 2. The flowchart of proposed model.

## 5- Simulation results

### 5-1- Data

The presented problem is investigated through four case studies, indicated in Table 2. As can be seen from this table, the effect of fixed and reconfigurable topologies as well as different objective functions on microgrid scheduling will be investigated. The generated scenarios for load demand, market price, solar radiation and wind speed are presented in Figs. 3a-3d, respectively. The scenarios presented in Fig. 3a are related to the fixed load of smart homes. It should be noted that the load of schedulable appliances will also be added to this load (depends on the activation time of appliances). As mentioned earlier, in order to reduce the computational burden, the number of scenarios of each uncertain parameter has been reduced to 10 by utilizing the SCENRED2 in GAMS, as illustrated in Figs. 4a-4d. The generated and reduced scenarios for traditional home demand are presented in Figs. 5a and 5b, respectively. The data of the modified IEEE 118-bus system are available in [47]. Furthermore, Tables 3 and 4 represent the data to model the microgrids and smart homes. Finally, the data required to simulate the problem are presented in Table 5.

Table 2. Case studies and their corresponding assumptions.

| Case no. | Topology | | Objective function | |
|---|---|---|---|---|
| | Fixed | Reconfigurable | Single-objective | Two-objective |
| **1** | ✓ | × | ✓ | × |
| **2** | × | ✓ | ✓ | × |
| **3** | ✓ | × | × | ✓ |
| **4** | × | ✓ | × | ✓ |

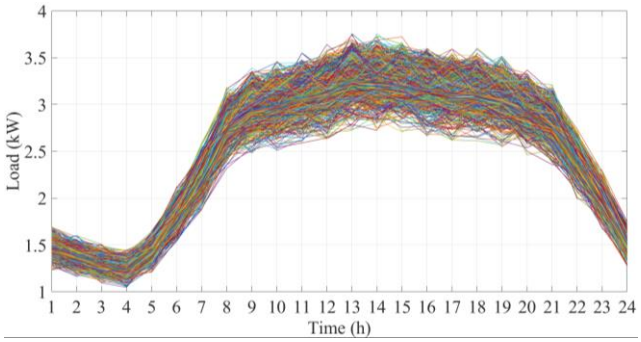


(a) Electrical load

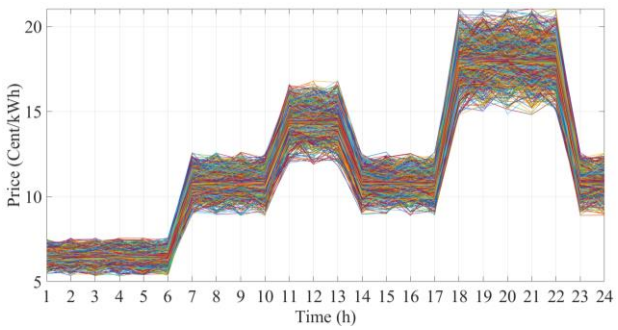


(b) Electricity price

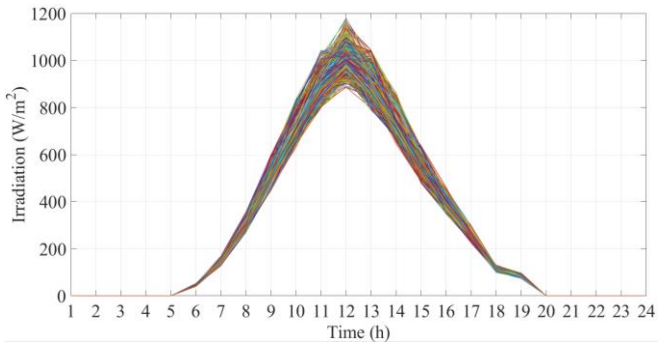


(c) Irradiance

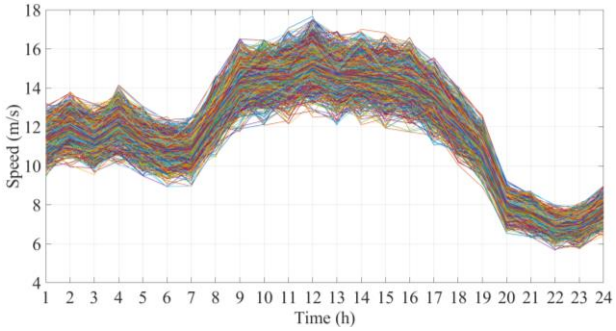


(d) Wind speed

Fig. 3. Generated scenarios for uncertain parameters.

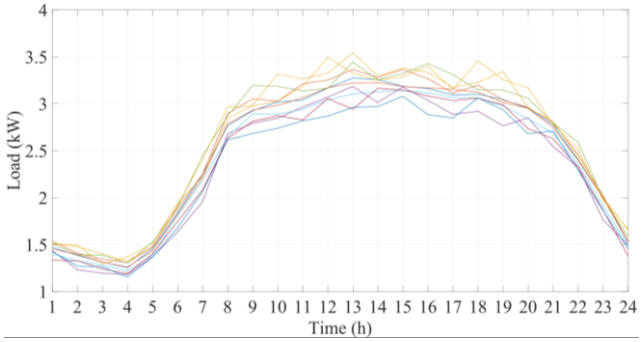


(a) Electrical load

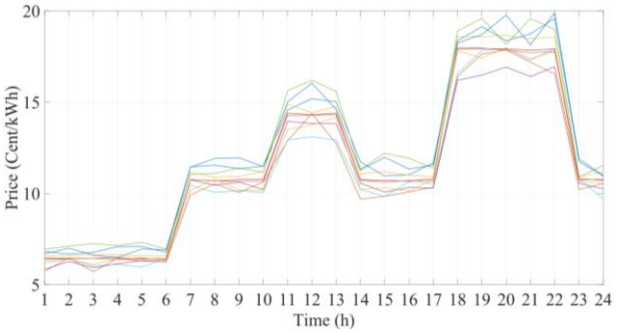


(b) Electricity price

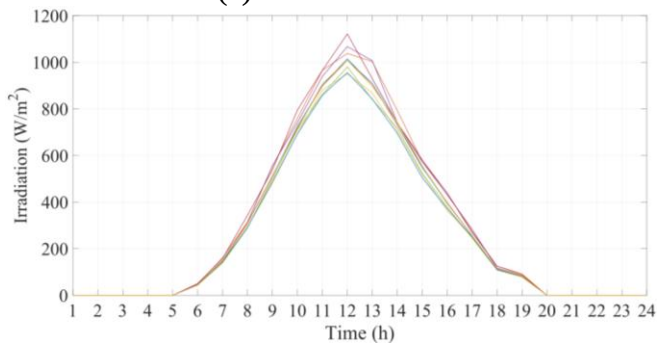


(c) Irradiance

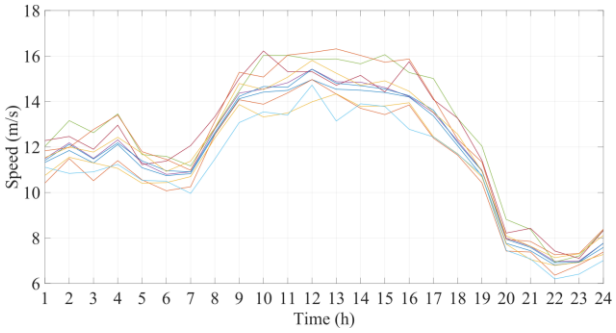


(d) Wind speed

Fig. 4. Reduced scenarios of uncertain parameters.

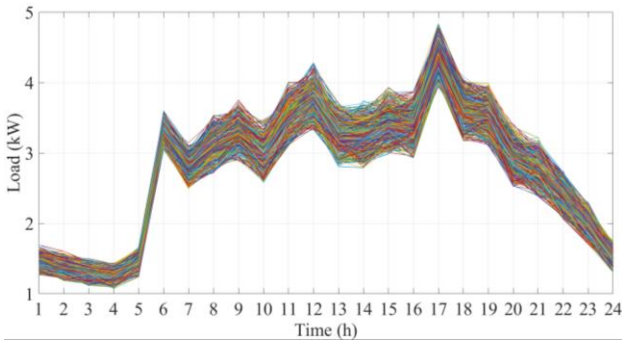


(a) Generated scenarios

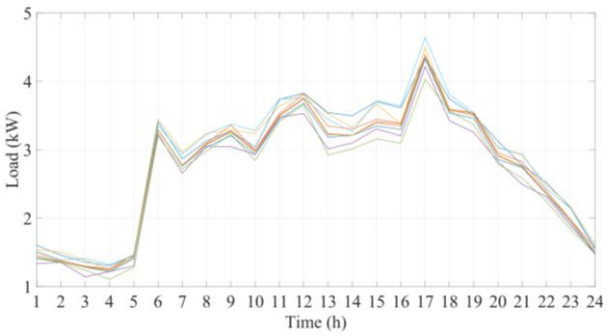


(b) Reduced scenarios

Fig. 5. Traditional home load scenarios

Table 3. Input data of microgrids.

| Microgrids No. | Number of Buses | Total Number of Customers | Number of Smart Homes | Capacity of DERs (kW) | |
|---|---|---|---|---|---|
| | | | | Gas Turbine | RER |
| 1 | 6 | 63 | 29 | 300 | - |
| 2 | 10 | 289 | 112 | 1000 | 1700 |
| 3 | 9 | 263 | 89 | 1200 | - |
| 4 | 13 | 791 | 110 | 2300 | 1000 |
| 5 | 8 | 314 | 188 | 900 | 1000 |
| 6 | 12 | 603 | 178 | 2600 | 500 |
| 7 | 8 | 235 | 78 | - | 2200 |
| 8 | 10 | 299 | 109 | - | 1600 |
| 9 | 9 | 605 | 107 | 2300 | - |
| 10 | 5 | 107 | 43 | 300 | - |

Table 4. Smart homes' appliance scheduling data.

| Appliance | UTR | PTR | LOT (h) | EEC (kWh) |
|---|---|---|---|---|
| **Washing Machine** | 9:00-17:00 | 10:00-11:00 | 2 | 1 |
| **Dishwasher** | 12:00-19:00 | 15:00-16:00 | 2 | 1.4 |
| **Clothes Dryer** | 11:00-19:00 | 12:00-13:00 | 1 | 1.8 |
| **Iron** | 5:00-9:00 | 6:00-7:00 | 1 | 1.1 |
| **Vacuum Cleaner** | 9:00-19:00 | 11:00-14:00 | 1 | 0.65 |
| **Microwave** | 11:00-16:00 | 13:00-14:00 | 1 | 0.9 |
| **Rice Cooker** | 10:00-15:00 | 12:00-13:00 | 2 | 0.6 |
| **Electric Kettle** | 6:00-10:00 | 7:00-8:00 | 1 | 1 |
| **Toaster** | 6:00-10:00 | 7:00-8:00 | 1 | 0.8 |

Table 5. Data required for simulation.

| Parameter | Value | Parameter | Value |
|---|---|---|---|
| $\pi_t^{e,\max}$ | 18 Cent | $\pi_g^{gen}$ | 6 Cent |
| $M$ | 1e7 | $v_i / v_r / v_o$ | 2 / 14 / 25 m/s |
| $N^{sw}$ | 40 | $G_{std}$ | 1000 W/m$^2$ |
| $\eta^{ch} / \eta^{dch}$ | 95% | $E_w^0 / E_{pv}^0$ | 20% |
| $\eta^{conv} / \eta_{pv}^{conv}$ | 95% | $E_w^{\min} / E_{pv}^{\min}$ | 20% |
| $\Delta t$ | 1 h | $E_w^{\max} / E_{pv}^{\max}$ | 100% |
| $V_{i,t,s}^{\min} / V_{i,t,s}^{\max}$ | 0.9 / 1.1 p.u. | $P_w^{ch,\max} / P_{pv}^{ch,\max}$ | 40% |
| $\theta_{i,t,s}^{\min} / \theta_{i,t,s}^{\max}$ | -3.14 / 3.14 rad | $P_w^{dch,\max} / P_{pv}^{dch,\max}$ | 40% |
| $T_{n_1,n_2}^{gap}$ | 1 h | $\eta^{gen}$ | 65% |

| | | | |
|---|---|---|---|
| $\beta_n$ | 1.1 | $\pi_w^{wind}$ / $\pi_{pv}^{solar}$ | 3 Cent |

Table 6 includes the results, obtained from solving the problem for the four case studies. As can be observed, the first iteration is associated with the best solution, since the scheduling problem of each microgrid is solved from its own point of view. Accordingly, the highest error also relates to this iteration. As the number of iterations increases, the error and the number of optimality cuts reduce, since the scheduling of microgrids would be more appropriately carried out by receiving the corrective signals from the DSO. It can be seen that the error and the number of optimality cuts reach zero in the last iteration. Thus, the obtained scheduling can be implemented. Errors are the difference between microgrids scheduling and DSO scheduling and are calculated in kW. For example, if microgrid 4 has a demand of 100 kW at 4 pm and DSO is only able to supply 60 kW of this demand due to network limitations, the error value will be equal to 40 kW. It should be noted that the value provided for the error in each iteration is the sum of the errors of all the optimality cuts in that iteration.

The comparison, made between Cases 2 & 4 and Cases 1 & 3 reveals that the DFR would lead to more reduced operating cost and enhanced consumers' comfort index. As Table 6 shows, operating cost in Case 2 decreased by 10.17% compared to Case 1, which is due to the implementation of DFR. The results also illustrate that the comfort index has increased by 2.9% compared to Case 1. Moreover, the deviation from the optimum scheduling of microgrids will be lower in Cases 2 and 4. This is due to the fact that the DSO reconfigures the system, aimed at minimizing the deviation from the optimum scheduling of microgrids. It can also be observed that the minimum operating cost relates to Case 2, as the objective in this case is minimizing the operating cost with the DFR possibility. A comparison of Cases 2 and 4 indicates that a 22.3% increase in the consumers' comfort index in case 4 has resulted in an increase of about 6.1% in operating costs.

Table 7 shows the final operation results, comprising the operating cost, consumers' comfort index, the amount of power transaction, the number of optimality cuts for each case and each microgrid. The obtained results also indicate that the DFR would more affect the operating cost of the microgrid than the comfort index. For instance, the operating cost of microgrid 2 in the first case study is 60.93 $/day, while in Case 2 with the DFR, microgrid 2 can make a profit by -1269.69 $/day through selling power to other microgrids. It is noted that this issue is adverse for some microgrids like microgrid 9 and microgrid 10, where their operating costs have relatively increased. In general, it can be concluded that the impact of the DFR on the operation of each microgrid is substantial.

Table 8 represents the hourly topology of the system with respect to the open switches for Case 2 and Case 4. It is worth noting that the system topology changes each hour as the state of open switches changes. The maximum number of switching is limited to 40 to avoid the amortization of switches and any noise in the system. Figs. 6a and 6b depict the number of switch changes per hour in Cases 2 and 4, respectively. As can be seen, the network topology in Case 4 has changed more than Case 2, which is due to the different objective functions of these cases. Finally, the obtained topologies for the network at different times of the day in Case 4 are presented in Figs. 7a-7d. It should be noted that the red dashed lines indicate the open switches. As can be seen, the network topology has changed at different times of the day in order to satisfy the objective functions.

Table 6. The obtained results of each case study.

| Iter. | Operation cost | | Comfort level | | Error (kW) | Number of cuts | |
|---|---|---|---|---|---|---|---|
| | Obtained ($/day) | Deviation from optimum point (%) | Obtained (%) | Deviation from optimum point (%) | | Positive cuts | Negative cuts |
| **Case study (1)** | | | | | | | |
| **1** | 8931.00 | 0 | 78.44 | 1.10 | 144150.7 | 230 | 170 |
| **2** | 10471.90 | 17.25 | 77.93 | 1.75 | 16040.30 | 54 | 37 |

| | | | | | | | |
|---|---|---|---|---|---|---|---|
| **3** | 10783.11 | 20.74 | 77.57 | 2.20 | 1130.78 | 18 | 5 |
| **4** | 10810.99 | 21.05 | 79.14 | 0.22 | 163.30 | 12 | 2 |
| **5** | 10815.66 | 21.10 | 79.32 | 0 | 66.90 | 9 | 0 |
| **6** | 10854.16 | 21.53 | 78.39 | 1.17 | 0 | 0 | 0 |
| **Case study (2)** | | | | | | | |
| **1** | 8929.41 | 0 | 80.05 | 2.92 | 75140.79 | 161 | 129 |
| **2** | 9431.08 | 5.62 | 80.04 | 2.93 | 23362.21 | 109 | 48 |
| **3** | 9573.56 | 7.21 | 80.14 | 2.81 | 7482.10 | 56 | 14 |
| **4** | 9583.94 | 7.33 | 80.07 | 2.90 | 1604.45 | 39 | 0 |
| **5** | 9589.40 | 7.39 | 82.03 | 0.52 | 1492.61 | 36 | 3 |
| **6** | 9593.53 | 7.44 | 82.46 | 0 | 1195.35 | 15 | 1 |
| **7** | 9664.65 | 8.23 | 81.46 | 1.21 | 532.62 | 7 | 3 |
| **8** | 9691.12 | 8.53 | 81.02 | 1.75 | 151.62 | 4 | 2 |
| **9** | 9750.43 | 9.19 | 80.73 | 2.10 | 0 | 0 | 0 |
| **Case study (3)** | | | | | | | |
| **1** | 10854.16 | 0 | 100 | 0 | 109612.4 | 170 | 146 |
| **2** | 11007.72 | 1.41 | 99.64 | 0.36 | 28675.33 | 50 | 39 |
| **3** | 11365.40 | 4.71 | 98.98 | 1.02 | 2798.40 | 12 | 9 |
| **4** | 11409.96 | 5.12 | 98.72 | 1.28 | 852.51 | 10 | 3 |
| **5** | 11437.25 | 5.37 | 98.68 | 1.32 | 432.22 | 7 | 11 |
| **6** | 11459.97 | 5.58 | 98.61 | 1.39 | 110.62 | 3 | 1 |
| **7** | 11468.40 | 5.66 | 98.58 | 1.42 | 0 | 0 | 0 |
| **Case study (4)** | | | | | | | |
| **1** | 9750.43 | 0 | 100 | 0 | 57097.04 | 122 | 108 |
| **2** | 10095.22 | 3.54 | 99.29 | 0.71 | 16774.64 | 68 | 36 |
| **3** | 10181.42 | 4.42 | 99.11 | 0.89 | 5179.51 | 43 | 23 |
| **4** | 10223.76 | 4.85 | 99.02 | 0.98 | 2516.33 | 13 | 11 |
| **5** | 10296.37 | 5.60 | 98.95 | 1.05 | 723.18 | 7 | 6 |
| **6** | 10308.65 | 5.73 | 98.87 | 1.13 | 529.11 | 9 | 5 |
| **7** | 10339.66 | 6.04 | 98.81 | 1.19 | 171.44 | 1 | 7 |
| **8** | 10353.82 | 6.19 | 98.76 | 1.24 | 0 | 0 | 0 |

Table 7. The obtained results of each microgrid in different case studies.

| Case (1) | | | | | | | Case (2) | | | | | | |
|---|---|---|---|---|---|---|---|---|---|---|---|---|---|
| **Microgrid No.** | **OC ($/day)** | **Comfort index (%)** | **Number of cuts** | | **Purchased power (kW)** | **Sold power (kW)** | **Microgrid No.** | **OC ($/day)** | **Comfort index (%)** | **Number of cuts** | | **Purchased power (kW)** | **Sold power (kW)** |
| | | | **Positive Cuts** | **Negative Cuts** | | | | | | **Positive Cuts** | **Negative Cuts** | | |
| **1** | 320.62 | 78.62 | 0 | 0 | 880.61 | 946.47 | **1** | 420.80 | 71.28 | 21 | 0 | 1899.70 | 213.47 |
| **2** | 60.93 | 76.76 | 72 | 5 | 0 | 5869.38 | **2** | -1269.69 | 85.78 | 67 | 41 | 0 | 27740.92 |
| **3** | 1184.59 | 76.76 | 31 | 30 | 3567.89 | 5889.88 | **3** | 1248.46 | 78.53 | 65 | 24 | 3516.02 | 5131.45 |
| **4** | 4255.62 | 80.39 | 23 | 49 | 10790.29 | 2318.67 | **4** | 4641.50 | 76.76 | 29 | 38 | 18123.97 | 0 |
| **5** | 226.80 | 78.53 | 2 | 23 | 816.95 | 6929.32 | **5** | 482.22 | 78.62 | 3 | 17 | 956.86 | 3447.15 |
| **6** | 2931.98 | 76.67 | 34 | 41 | 5600.00 | 5426.45 | **6** | 2747.60 | 83.92 | 42 | 15 | 7471.34 | 9314.39 |
| **7** | -1881.26 | 80.39 | 51 | 2 | 0 | 23834.44 | **7** | -1948.29 | 85.78 | 95 | 12 | 21.32 | 25552.92 |
| **8** | 7.43 | 80.29 | 50 | 21 | 0 | 6096.59 | **8** | -465.79 | 84.02 | 38 | 10 | 76.98 | 11519.18 |
| **9** | 3071.02 | 78.62 | 42 | 24 | 8398.55 | 2431.51 | **9** | 3208.29 | 84.02 | 27 | 16 | 9836.94 | 1613.55 |
| **10** | 676.43 | 76.86 | 18 | 19 | 2586.09 | 1.36 | **10** | 685.33 | 78.62 | 40 | 27 | 2942.37 | 0 |
| **Case (3)** | | | | | | | **Case (4)** | | | | | | |
| **Microgrid No.** | **OC ($/day)** | **Comfort index (%)** | **Positive Cuts** | **Negative Cuts** | **Purchased power (kW)** | **Sold power (kW)** | **Microgrid No.** | **OC ($/day)** | **Comfort index (%)** | **Positive Cuts** | **Negative Cuts** | **Purchased power (kW)** | **Sold power (kW)** |
| **1** | 356.18 | 100 | 0 | 0 | 1861.36 | 425.56 | **1** | 367.81 | 100 | 0 | 0 | 1915.43 | 505.80 |
| **2** | 91.40 | 100 | 72 | 3 | 0 | 5853.17 | **2** | -1227.00 | 100 | 55 | 31 | 0 | 27884.75 |
| **3** | 1239.30 | 96.47 | 28 | 28 | 3676.66 | 5615.80 | **3** | 1320.45 | 100 | 36 | 38 | 3236.62 | 4215.25 |
| **4** | 4380.45 | 100 | 11 | 49 | 11046.38 | 1686.81 | **4** | 4714.91 | 100 | 26 | 29 | 22091.07 | 0 |
| **5** | 366.93 | 96.47 | 7 | 23 | 1171.48 | 5761.10 | **5** | 432.37 | 96.47 | 10 | 13 | 1092.13 | 4965.08 |
| **6** | 3011.17 | 100 | 16 | 45 | 5600.00 | 5426.45 | **6** | 2898.00 | 98.23 | 37 | 28 | 7475.44 | 7256.73 |
| **7** | -1830.49 | 96.47 | 32 | 4 | 0 | 23220.04 | **7** | -1754.50 | 100.00 | 37 | 14 | 0 | 24659.02 |
| **8** | 17.37 | 100 | 52 | 12 | 0 | 6037.37 | **8** | -413.77 | 98.23 | 34 | 8 | 273.77 | 11327.56 |
| **9** | 3135.20 | 96.47 | 20 | 24 | 9441.12 | 2236.26 | **9** | 3301.20 | 94.70 | 14 | 13 | 10716.22 | 1300.86 |
| **10** | 700.89 | 100 | 14 | 21 | 3148.64 | 0 | **10** | 714.36 | 100 | 14 | 22 | 3395.86 | 0 |

Table 8. The obtained topology in cases 2 and 4.

| Hour | Open Switches | |
|---|---|---|
| | Case 2 | Case 4 |
| 1 | $S_1,S_2,S_3,S_4,S_5,S_7,S_{13},S_{14},S_{15}$ | $S_1,S_2,S_3,S_4,S_6,S_7,S_9,S_{10},S_{14}$ |
| 2 | $S_1,S_2,S_3,S_4,S_5,S_7,S_{13},S_{14},S_{15}$ | $S_1,S_2,S_3,S_4,S_6,S_7,S_9,S_{10},S_{14}$ |
| 3 | $S_1,S_2,S_3,S_4,S_7,S_{10},S_{13},S_{14},S_{15}$ | $S_1,S_2,S_3,S_4,S_6,S_7,S_9,S_{10},S_{14}$ |
| 4 | $S_1,S_2,S_3,S_4,S_7,S_{10},S_{13},S_{14},S_{15}$ | $S_1,S_2,S_3,S_4,S_6,S_7,S_9,S_{10},S_{14}$ |
| 5 | $S_1,S_2,S_3,S_4,S_7,S_{10},S_{13},S_{14},S_{15}$ | $S_1,S_2,S_3,S_4,S_6,S_7,S_8,S_{10},S_{14}$ |
| 6 | $S_1,S_2,S_3,S_4,S_5,S_7,S_{10},S_{14},S_{15}$ | $S_1,S_2,S_3,S_4,S_5,S_7,S_8,S_{13},S_{14}$ |
| 7 | $S_1,S_2,S_3,S_4,S_5,S_7,S_{11},S_{14},S_{15}$ | $S_1,S_2,S_3,S_4,S_5,S_7,S_8,S_{13},S_{14}$ |
| 8 | $S_1,S_2,S_3,S_4,S_5,S_7,S_{11},S_{14},S_{15}$ | $S_1,S_2,S_3,S_4,S_5,S_7,S_9,S_{10},S_{14}$ |
| 9 | $S_1,S_2,S_3,S_4,S_5,S_7,S_{11},S_{14},S_{15}$ | $S_1,S_2,S_3,S_4,S_5,S_7,S_9,S_{10},S_{14}$ |
| 10 | $S_1,S_2,S_3,S_4,S_5,S_7,S_{11},S_{14},S_{15}$ | $S_1,S_2,S_3,S_4,S_5,S_7,S_9,S_{10},S_{14}$ |
| 11 | $S_1,S_2,S_3,S_4,S_5,S_7,S_{11},S_{14},S_{15}$ | $S_1,S_2,S_3,S_4,S_7,S_9,S_{10},S_{11},S_{14}$ |
| 12 | $S_1,S_2,S_3,S_4,S_5,S_7,S_{11},S_{14},S_{15}$ | $S_1,S_2,S_3,S_4,S_7,S_9,S_{10},S_{11},S_{14}$ |
| 13 | $S_1,S_2,S_3,S_4,S_5,S_7,S_{11},S_{14},S_{15}$ | $S_1,S_2,S_3,S_4,S_7,S_9,S_{10},S_{11},S_{14}$ |
| 14 | $S_1,S_2,S_3,S_4,S_5,S_7,S_{11},S_{14},S_{15}$ | $S_1,S_2,S_3,S_4,S_5,S_7,S_9,S_{11},S_{14}$ |
| 15 | $S_1,S_2,S_3,S_4,S_5,S_7,S_{11},S_{14},S_{15}$ | $S_1,S_2,S_3,S_4,S_5,S_7,S_9,S_{11},S_{14}$ |
| 16 | $S_1,S_2,S_3,S_4,S_5,S_7,S_{11},S_{14},S_{15}$ | $S_1,S_2,S_3,S_4,S_5,S_7,S_9,S_{11},S_{14}$ |
| 17 | $S_1,S_2,S_4,S_5,S_7,S_8,S_{11},S_{12},S_{14}$ | $S_1,S_2,S_4,S_5,S_7,S_9,S_{11},S_{12},S_{14}$ |
| 18 | $S_1,S_2,S_4,S_7,S_9,S_{10},S_{11},S_{12},S_{14}$ | $S_1,S_2,S_3,S_4,S_7,S_{10},S_{12},S_{14},S_{15}$ |
| 19 | $S_1,S_2,S_4,S_5,S_7,S_{10},S_{12},S_{14},S_{15}$ | $S_1,S_2,S_3,S_4,S_7,S_8,S_{10},S_{12},S_{14}$ |
| 20 | $S_1,S_2,S_4,S_5,S_7,S_{10},S_{12},S_{14},S_{15}$ | $S_1,S_2,S_3,S_4,S_7,S_8,S_{10},S_{12}S_{14}$ |
| 21 | $S_1,S_2,S_4,S_5,S_7,S_{10},S_{12},S_{14},S_{15}$ | $S_1,S_2,S_3,S_4,S_7,S_8,S_{10},S_{13},S_{14}$ |
| 22 | $S_1,S_2,S_4,S_5,S_6,S_7,S_{10},S_{14},S_{15}$ | $S_1,S_2,S_3,S_4,S_7,S_8,S_{10},S_{13},S_{14}$ |
| 23 | $S_1,S_2,S_3,S_4,S_8,S_9,S_{10},S_{13},S_{14}$ | $S_1,S_2,S_3,S_4,S_5,S_7,S_8,S_{10},S_{14}$ |
| 24 | $S_1,S_2,S_3,S_4,S_8,S_9,S_{10},S_{13},S_{14}$ | $S_1,S_2,S_3,S_5,S_7,S_8,S_{10},S_{13},S_{14}$ |

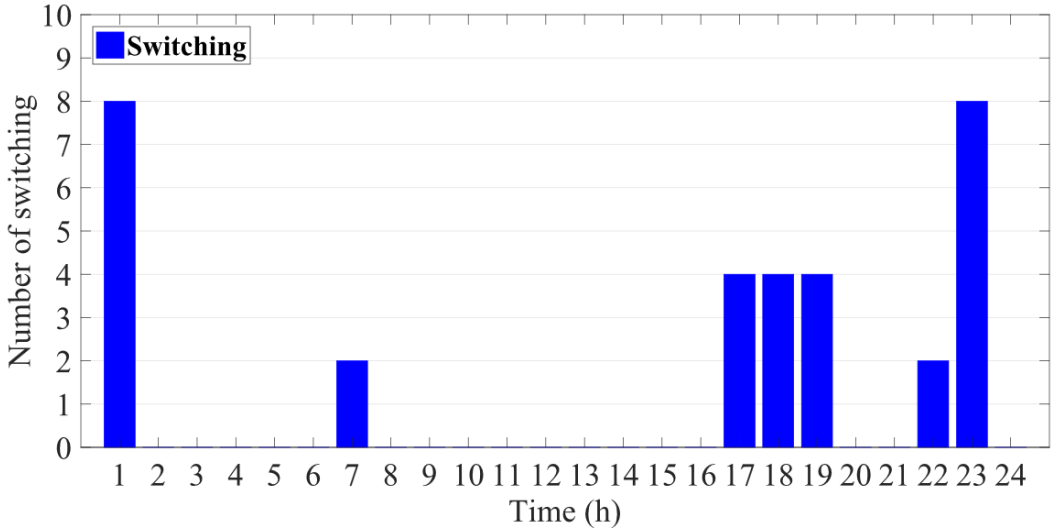


(a) Case 2

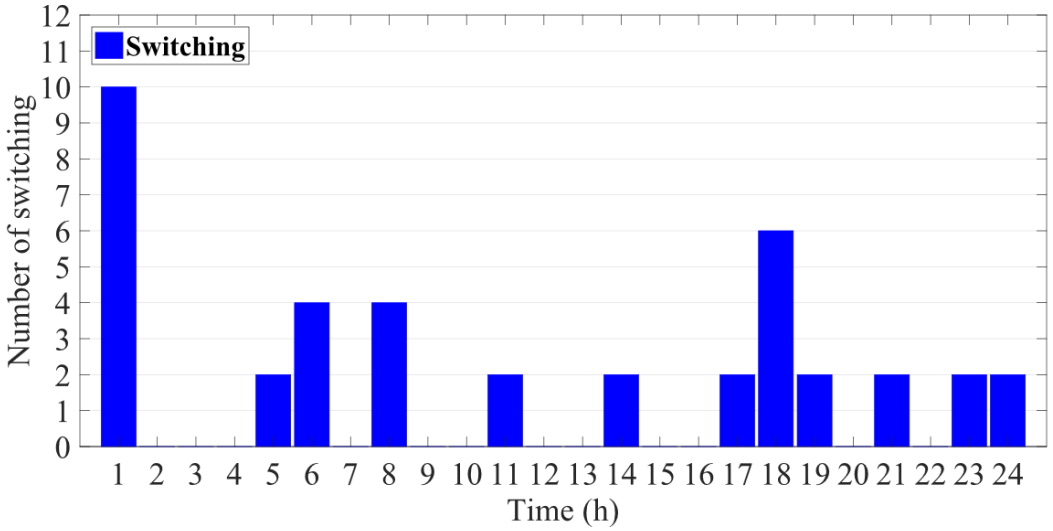


(b) Case 4

Fig. 6. The hourly switching in cases 2 and 4.

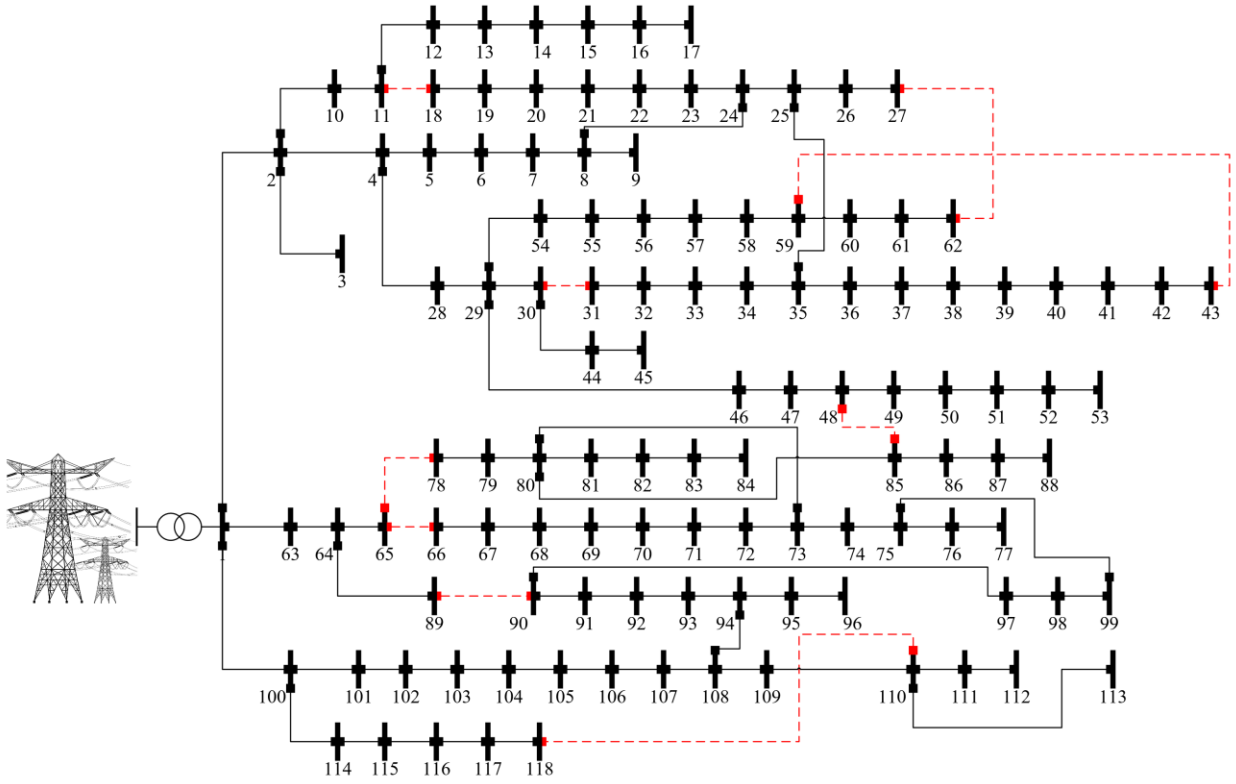

(a) Network topology at 10 a.m.

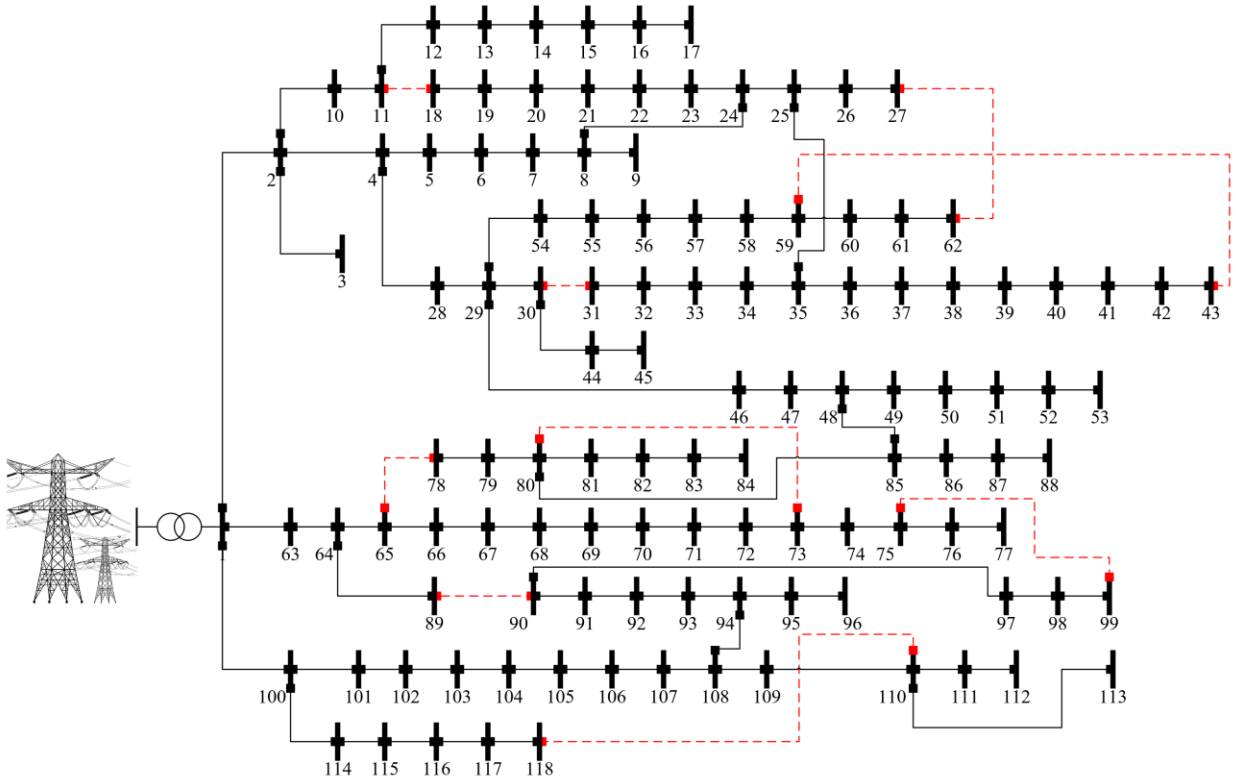


(b) Network topology at 17 p.m.

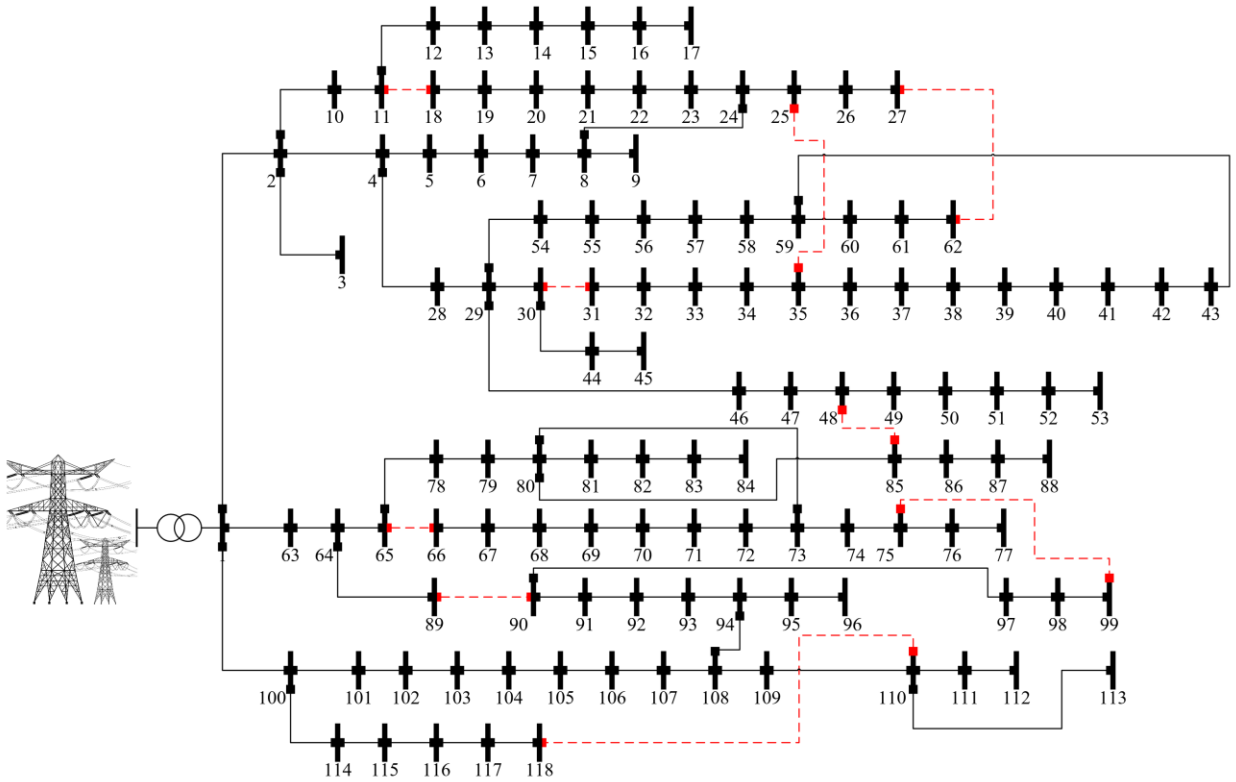

(c) Network topology at 18 p.m.

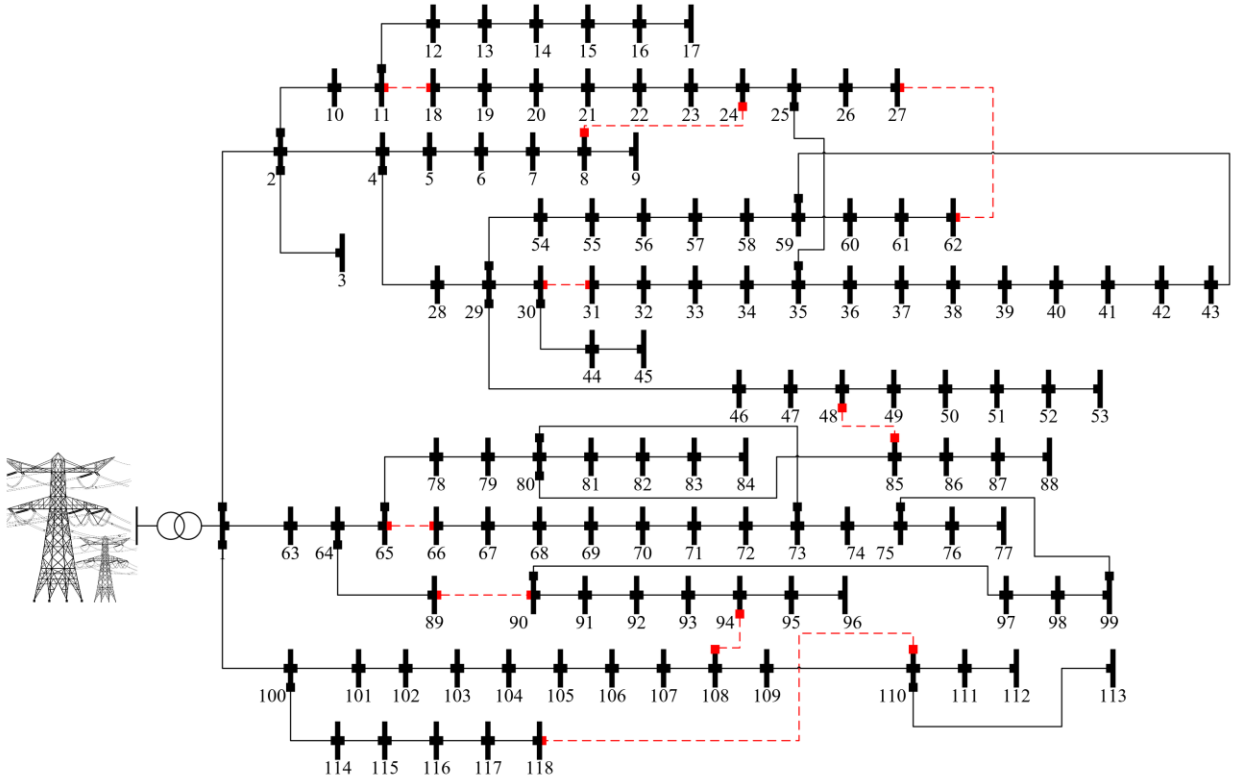


(d) Network topology at 21 p.m.

Fig. 7. Different topologies obtained for the network in case 4.

Figs. 8a-8d illustrates the system voltage in per unit (p.u.) for different case studies through box plots. The allowable range of voltage variation is considered to be + or -10% (between 0.9 p.u. to 1.1 p.u.). As these figures depict, the voltage has remained within the permitted range in all cases. The results, obtained in Cases 2 and 4 show that the DFR and increased local power generation have all led to the lower voltage drop over the initial hours, compared to Cases 1 and 3. Besides, the outliers in Cases 1 and 3 indicate that the voltage fluctuation is much more in comparison with the other two case studies. The hourly aggregated power, generated by DERs in the four case studies, is demonstrated in Figs. 9a and 9b. As can be observed, the amount of power, produced by DERs in Cases 2 and 4 is higher than Cases 1 and 3. The analysis of Fig. 9a illustrates that the

power generated by DERs during the operation period (24 hours) in Cases 1 and 2 are 289.326 MW and 295.773 MW, respectively, which shows a 2.23% increase in generation due to the use of DFR. Besides, a closer look at Fig. 9b indicates that the power generated by DERs in Cases 3 and 4 are 287.622 MW and 294.461 MW, respectively. Therefore, in these cases, the high effect of DFR on increasing the generation of DERs is proved. It should be noted that the implementation of DFR allows the exchange of power between microgrids in many hours in Cases 2 and 4. While in Cases 1 and 3, it is not possible for microgrids to transact power over some hours due to the topological limitations of the system. Thus, microgrids transact power only with the upstream network.

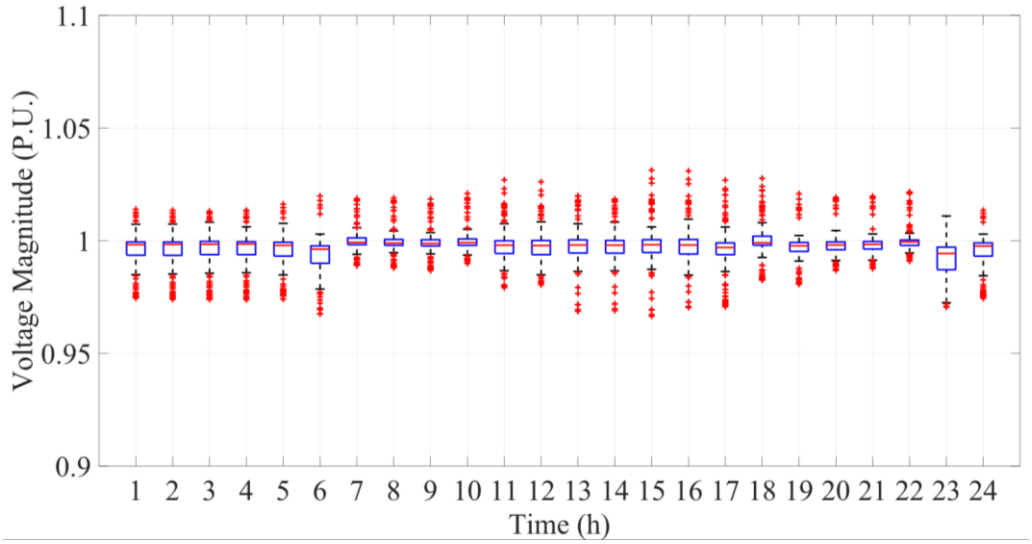


(a) Case 1

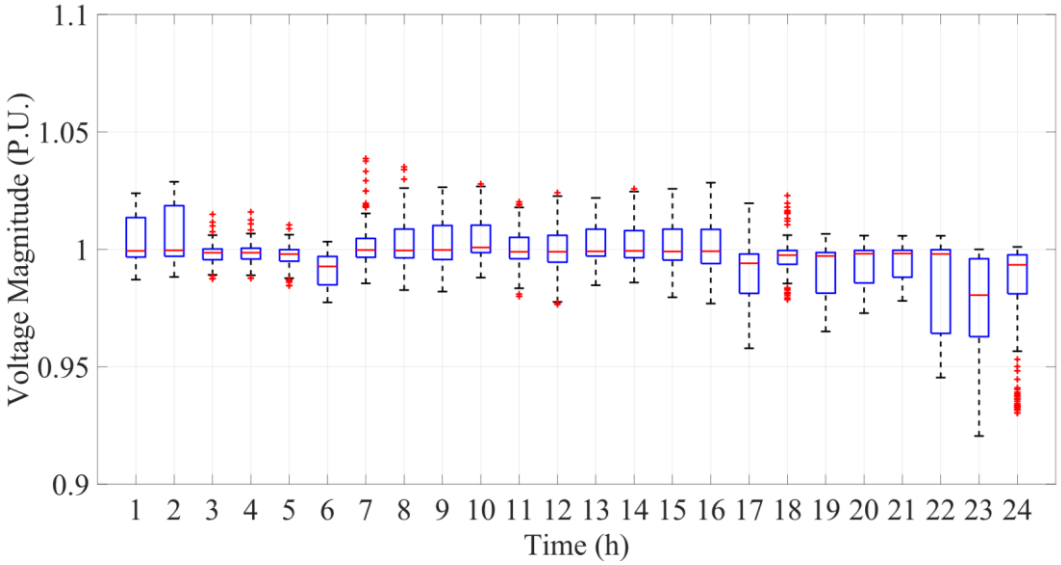


(b) Case 2

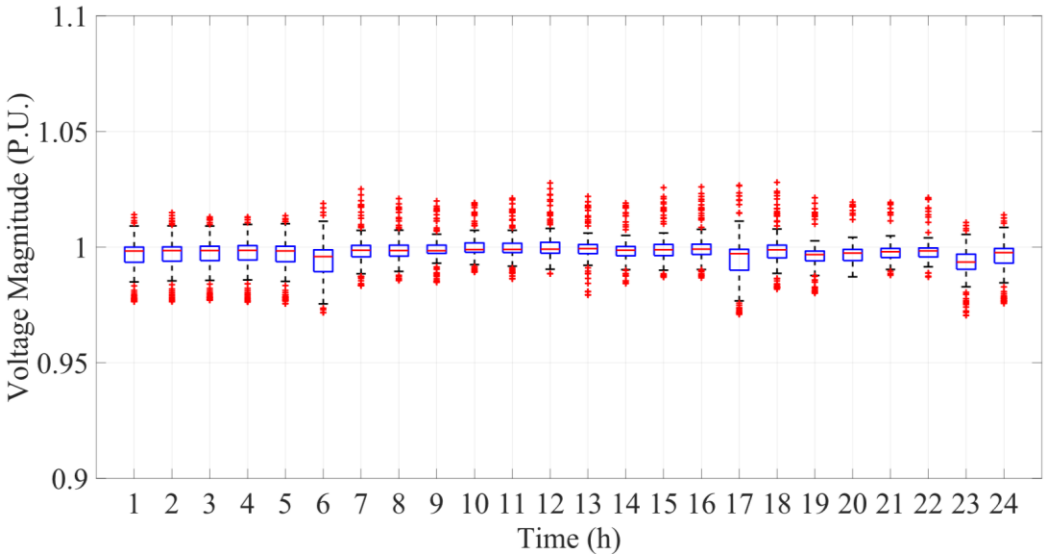


(c) Case 3

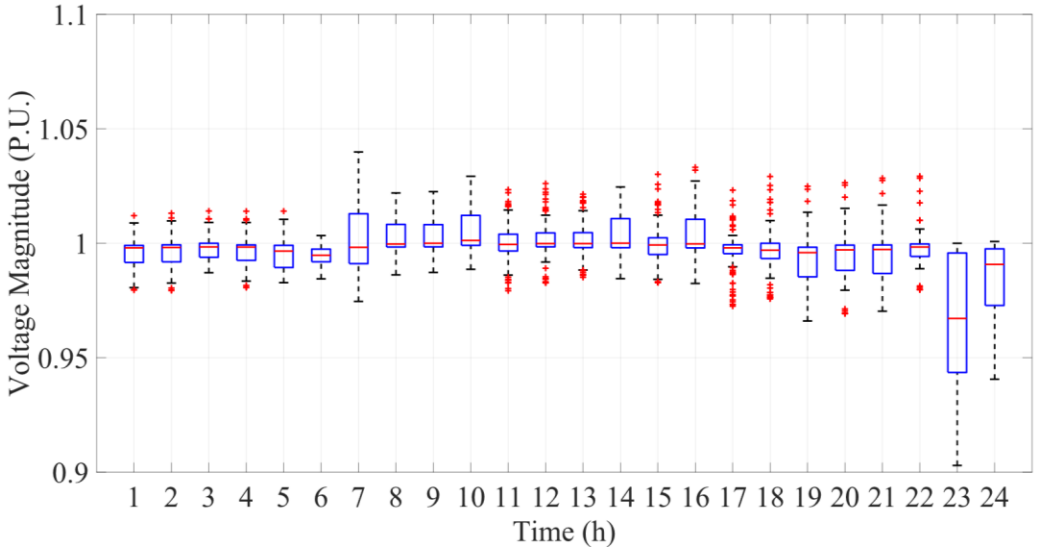


(d) Case 4

Fig. 8. The voltage magnitude at each hour.

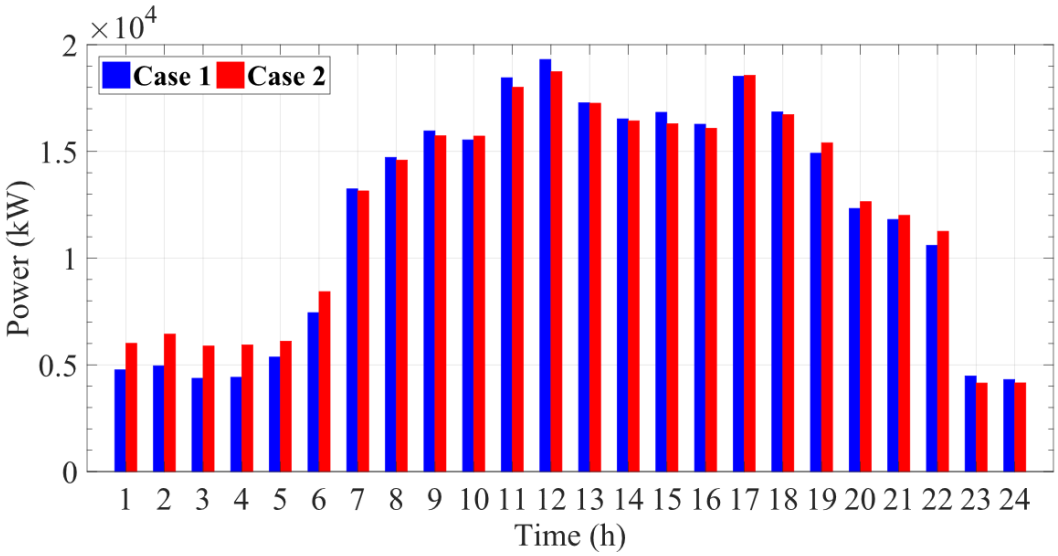


(a) Cases 1 and 2

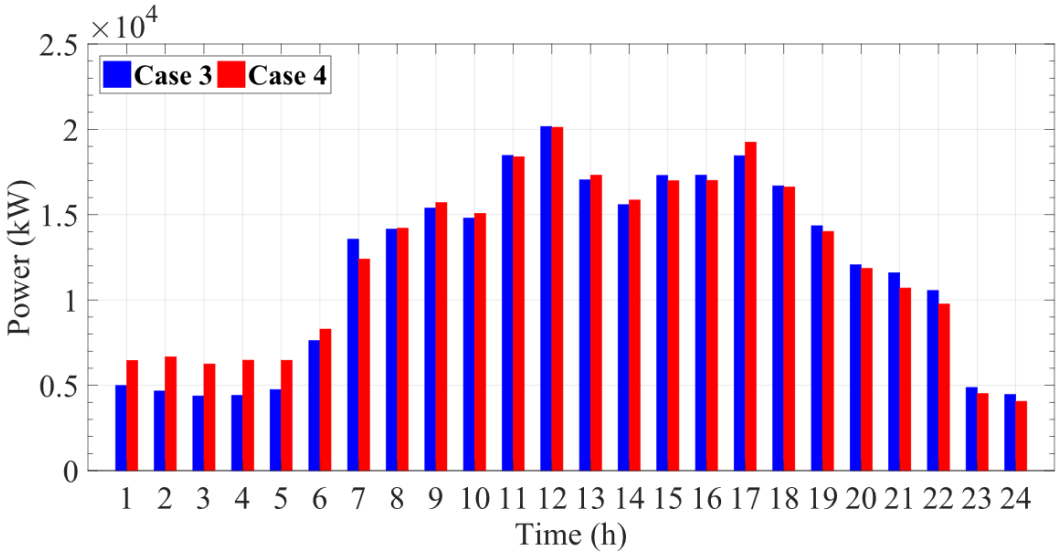


(b) Cases 3 and 4

Fig. 9. Total power generated by DERs in different cases.

Figs. 10a-10d depict the optimal scheduling of a smart home, located in microgrid 3 for the four case studies. As can be seen, in Cases 1 and 2, some devices are not activated in the customers' preferred range (presented in Table 4), while in case 3, only two appliances (electric kettle and toaster) are not activated in the customers' preferred range. This is due to the consumers' comfort index being considered as one of the objective functions. As can be seen from Fig. 10d, the comfort index of the smart homes located in microgrid 3 is 100% in Case 4 and the scheduling is quite in accordance with the consumer's preferences. The schedules obtained for smart homes located on other microgrids are presented in appendix (Figs. 12-20).

Figs. 11a-11j depict the operating points of smart homes' EES systems. As can be seen, the operating points of all systems are almost the same. According to the figures, these systems are charged during off-peak hours and discharged during peak hours. In general, this performance reduces the purchase of power during peak hours and consequently reduces the cost of electricity bills.

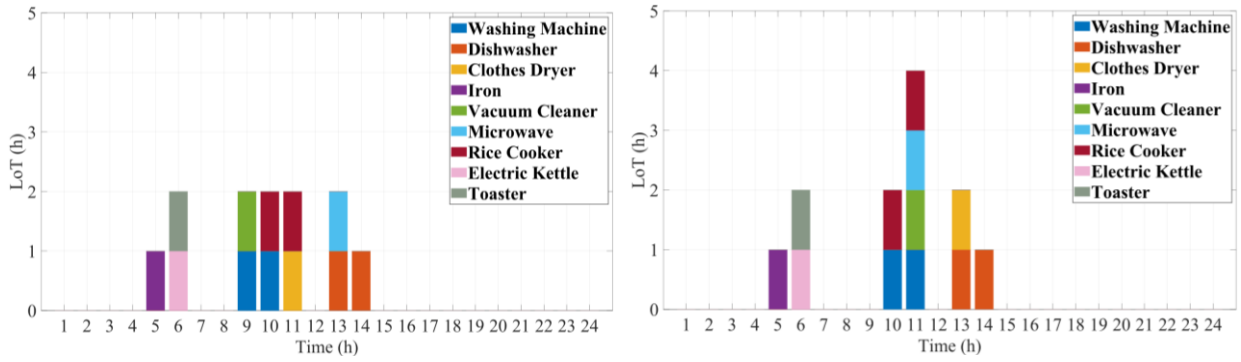


(a) Case 1




(b) Case 2

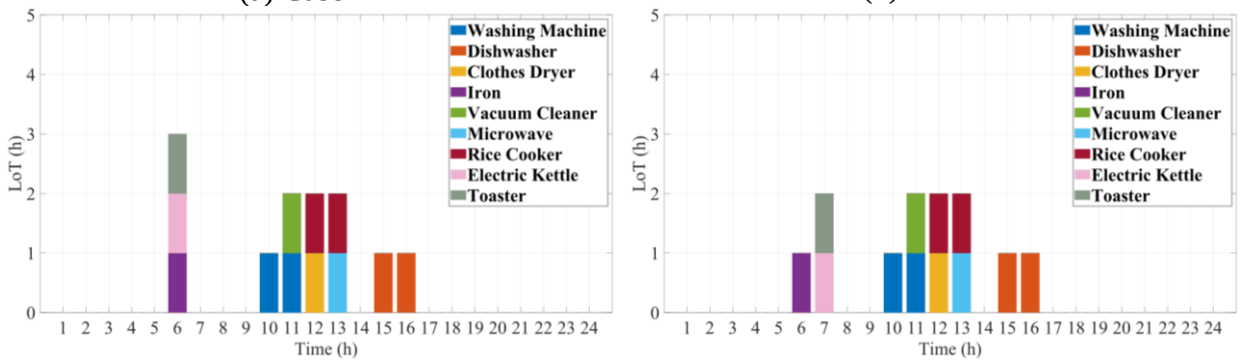


(c) Case 3




(d) Case 4

Fig. 10. The obtained scheduling for a smart home in microgrid 3.

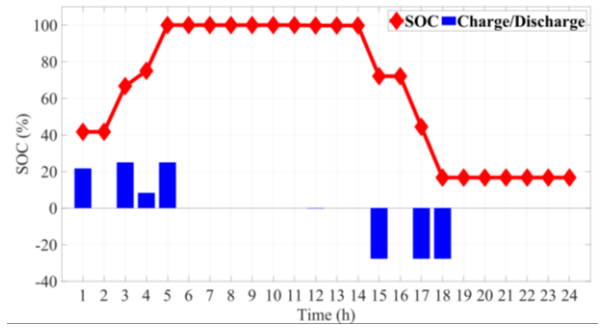


(a) EES system at node 14

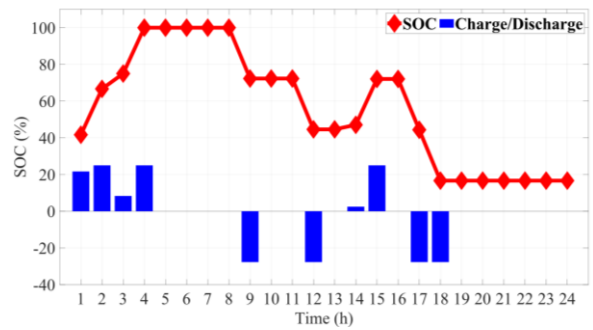


(b) EES system at node 20

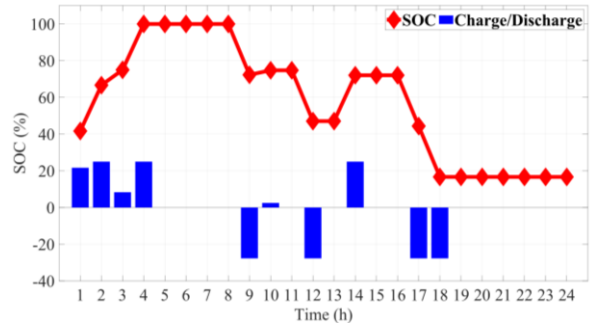


(c) EES system at node 54

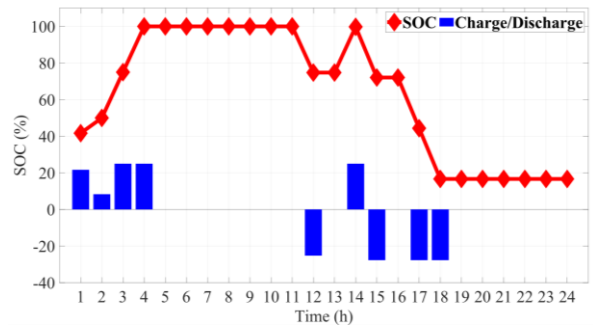


(d) EES system at node 42

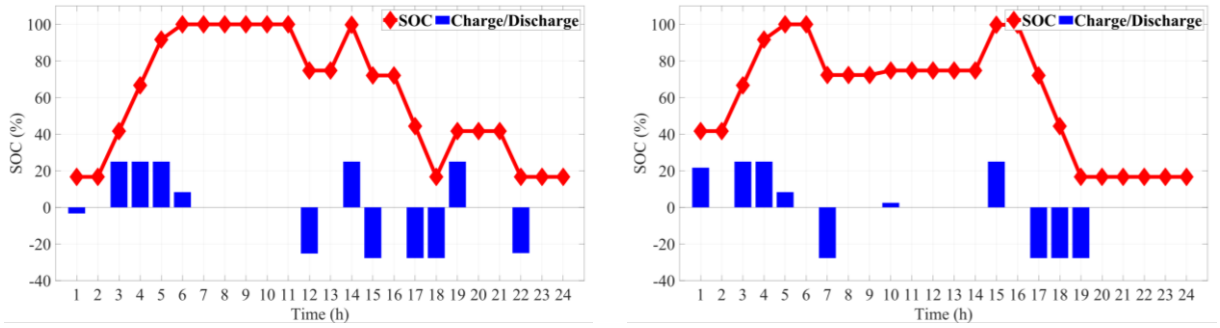


(e) EES system at node 50




(f) EES system at node 86

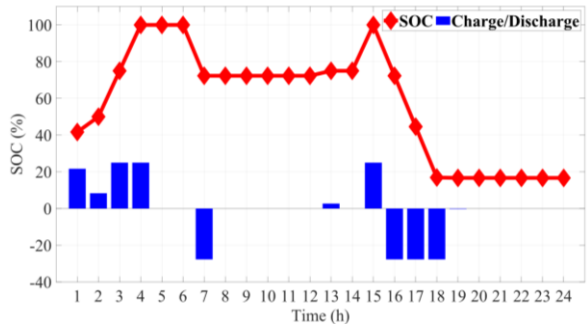


(g) EES system at node 74

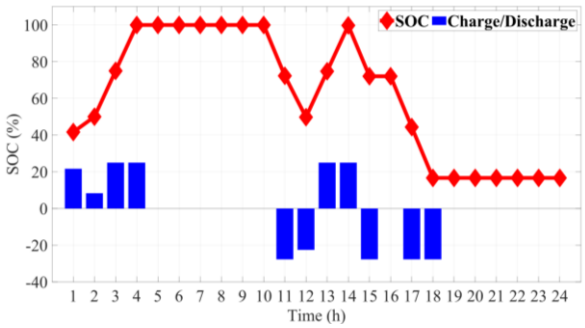


(h) EES system at node 96

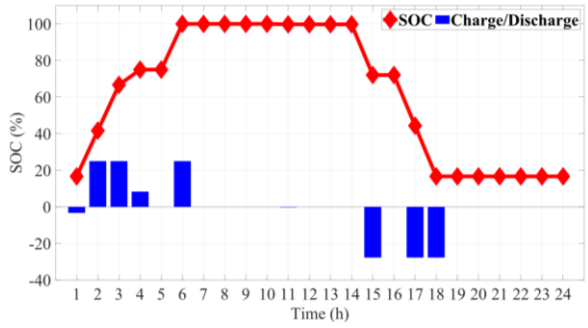


(i) EES system at node 102

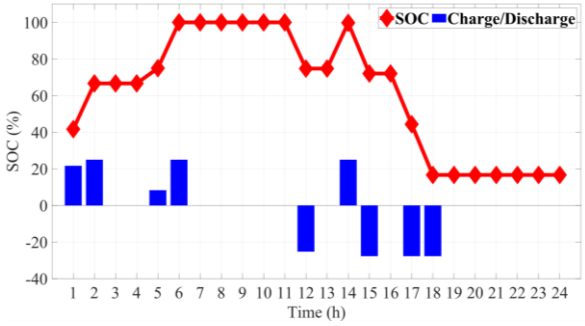


(j) EES system at node 114

Fig. 11. The operating point of EES systems located in smart homes.

## 6- Conclusion

This paper presents a two-stage stochastic MILP framework for energy management of active distribution systems consisting of interconnected microgrids. The network studied in this paper was a modified 118-bus radial distribution system consisting of 10 microgrids in which traditional loads and smart homes were considered. In the proposed model, DSO performed the main grid scheduling with observance of optimal scheduling of microgrids and with the possibility of DFR

implementation. Finally, the model was solved in the form of 4 case studies and the results are summarized as follows:

- Microgrid scheduling problem was solved with both single-objective and two-objective methods and the results mirrored that the use of two-objective method despite a 5.65% increase in operating costs led to a significant increase in consumer's comfort index.
- The main grid scheduling problem was solved by considering both fixed and dynamic topologies and the results illustrated that automatic switching reduced the total operating cost by 9.71% and increased the consumer's comfort index by about 0.2%. In addition, the results mirrored that automatic switching reduces the final scheduling deviation of microgrids from their optimal program.
- Examination of the operating point of EES systems demonstrated that these systems were charged during off-peak hours when the price of electricity was cheap and discharged during peak hours when the price of electricity was high, thus reducing operating costs.

Overall, the results proved that the two-level model proposed in this paper is an optimal framework for managing distribution systems consisting of interconnected microgrids.

**Acknowledgement**

M.S. Javadi and J.P.S. Catalão acknowledge the support by FEDER funds through COMPETE 2020 and by Portuguese funds through FCT, under 02/SAICT/2017 (POCI-01-0145-FEDER-029803).

**Appendix**

The schedules obtained for the smart homes in different microgrids are provided in Figs. 12-20.

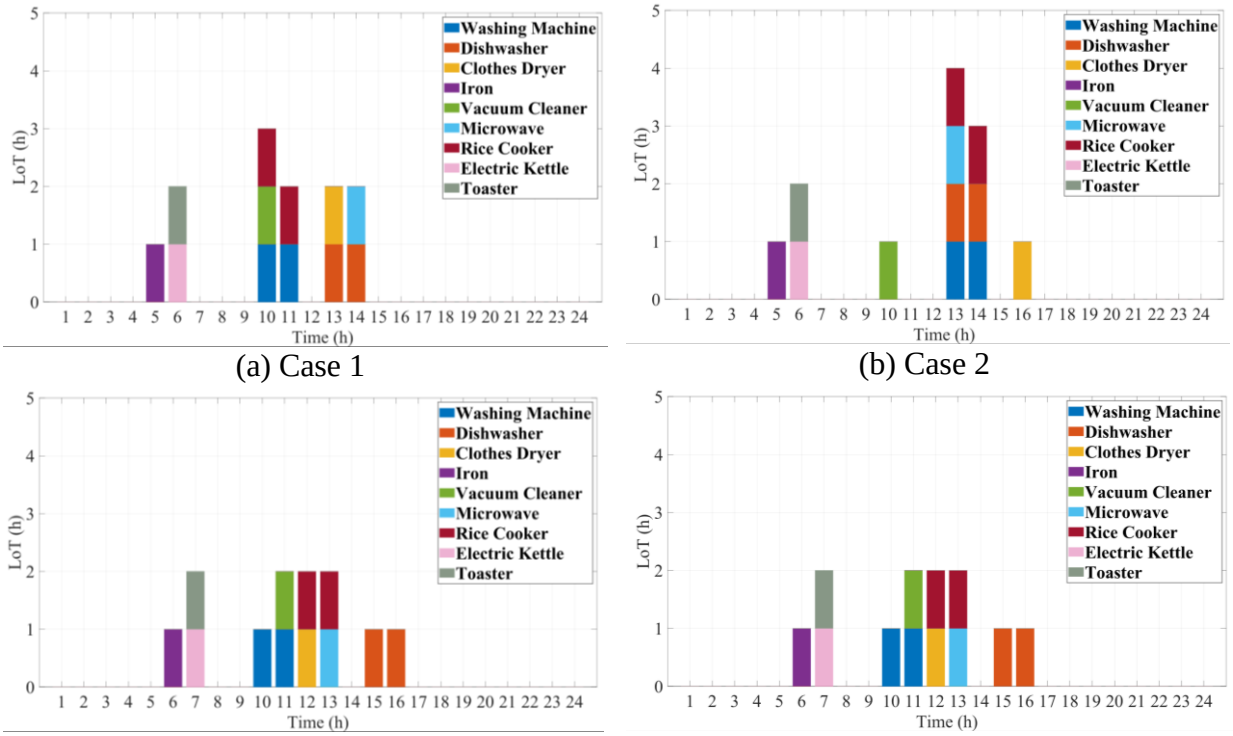


(a) Case 1 (b) Case 2

(c) Case 3 (d) Case 4

Fig. 12. The obtained scheduling for a smart home in microgrid 1.

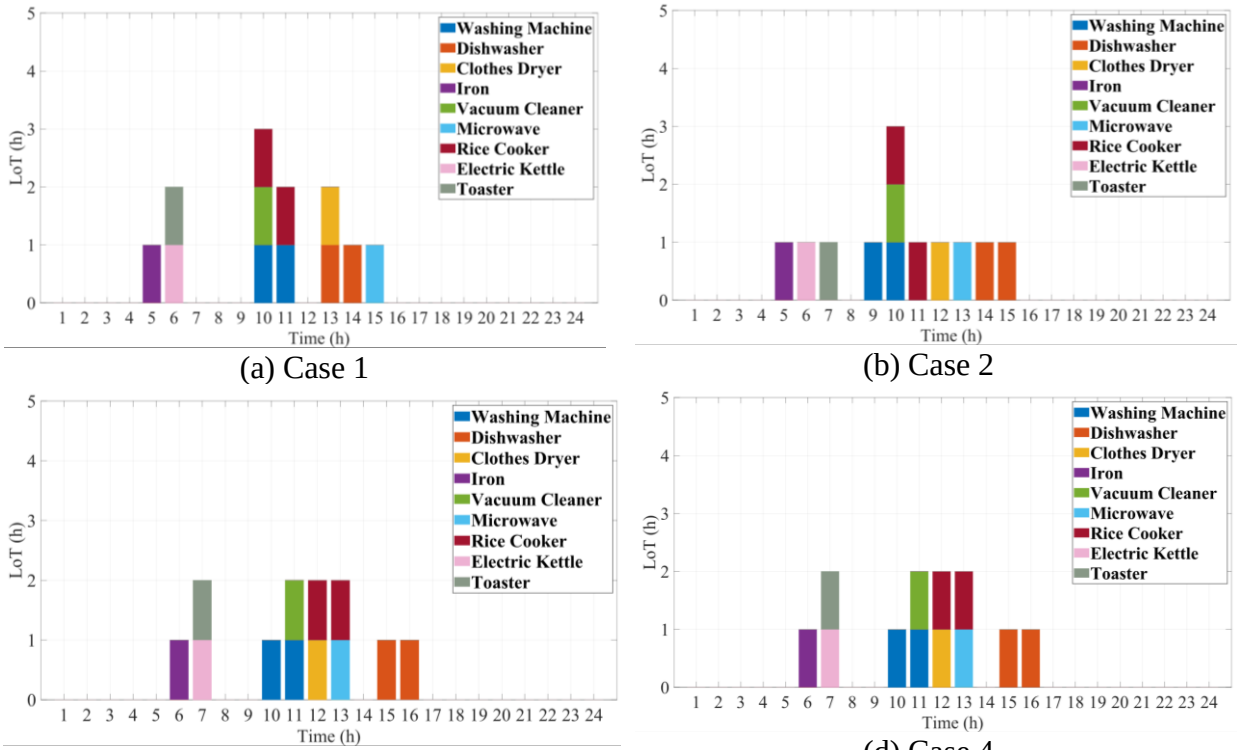


(a) Case 1 (b) Case 2

(c) Case 3 (d) Case 4

Fig. 13. The obtained scheduling for a smart home in microgrid 2.

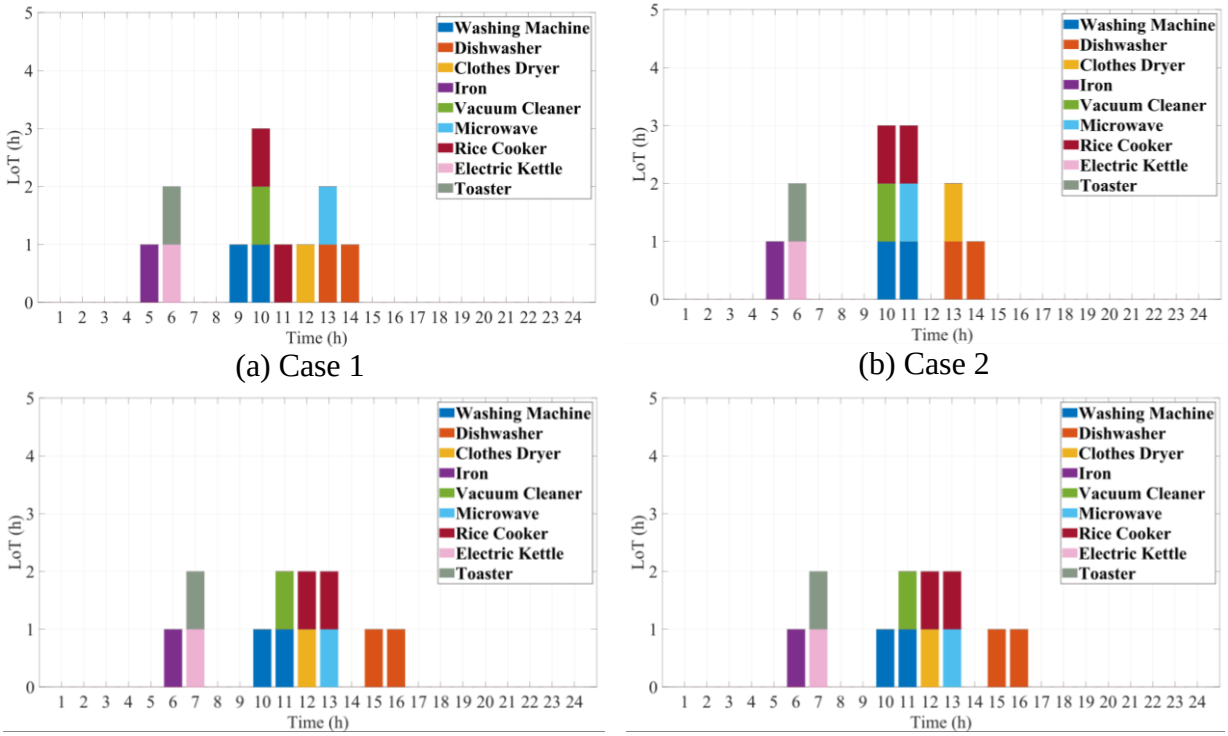


(a) Case 1 (b) Case 2

(c) Case 3 (d) Case 4

Fig. 14. The obtained scheduling for a smart home in microgrid 4.

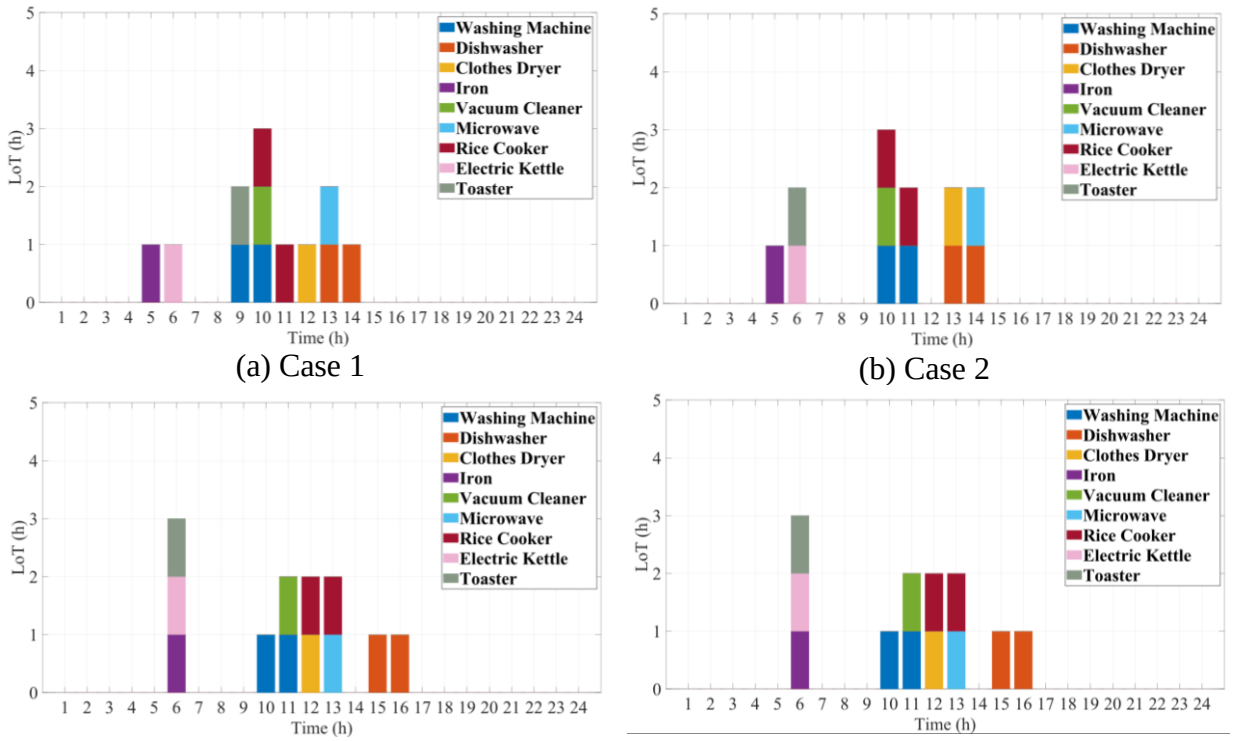


(a) Case 1 (b) Case 2

(c) Case 3 (d) Case 4

Fig. 15. The obtained scheduling for a smart home in microgrid 5.

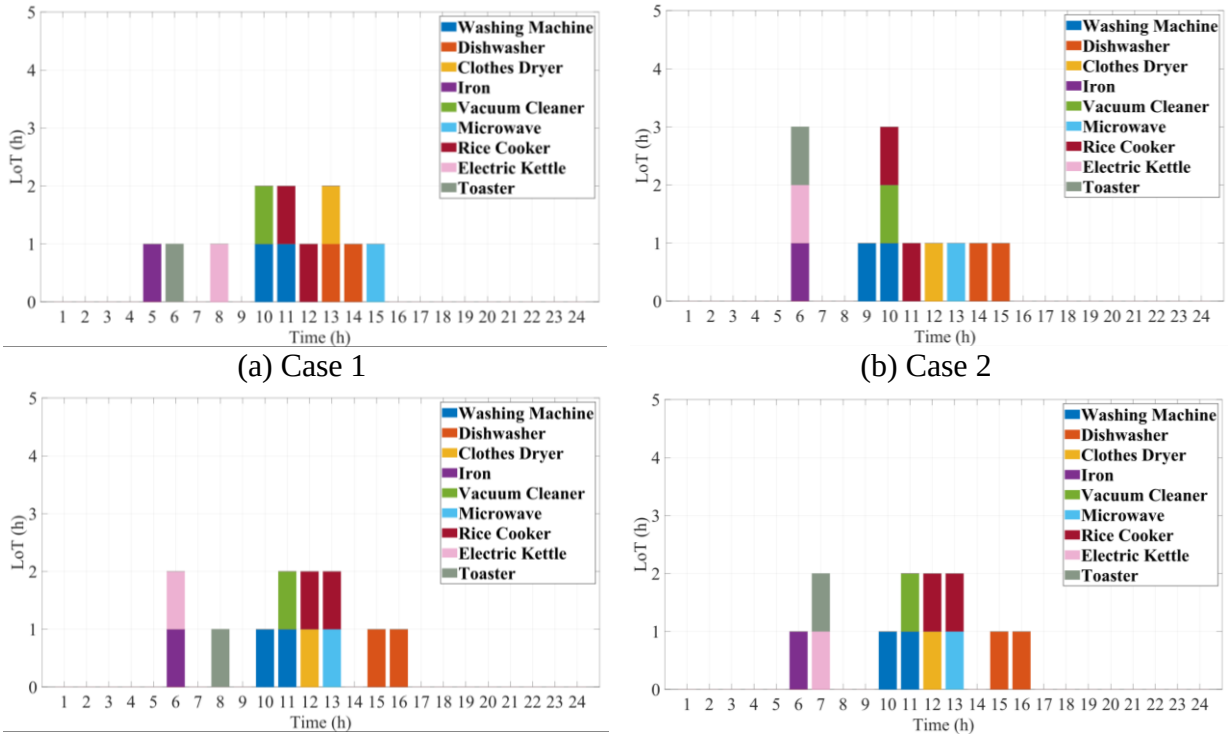


(a) Case 1 (b) Case 2

(c) Case 3 (d) Case 4

Fig. 16. The obtained scheduling for a smart home in microgrid 6.

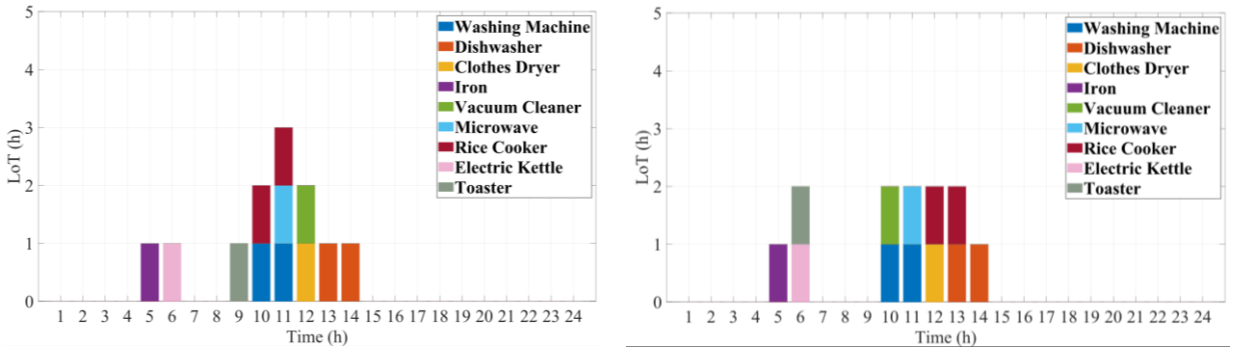


(a) Case 1 (b) Case 2

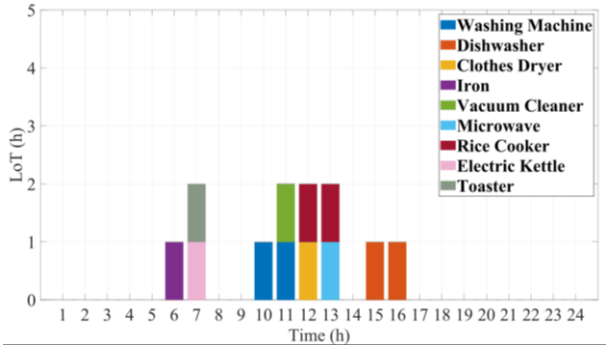


(c) Case 3

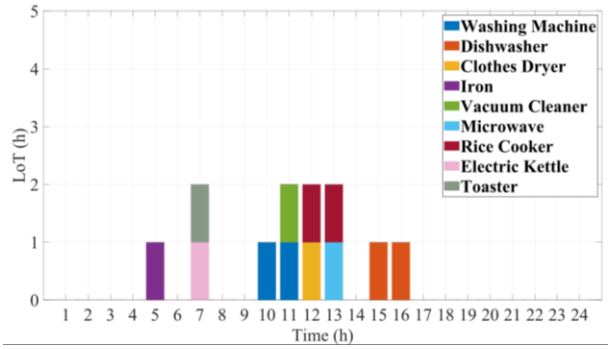


(d) Case 4

Fig. 17. The obtained scheduling for a smart home in microgrid 7.

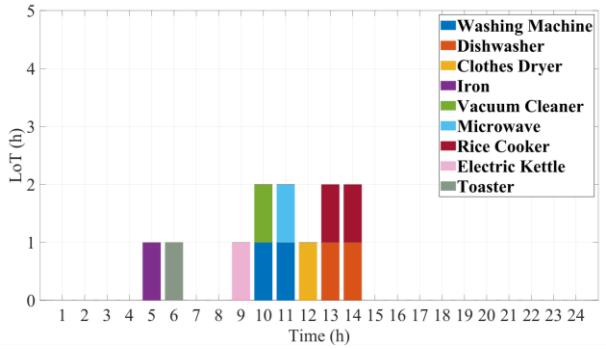


(a) Case 1

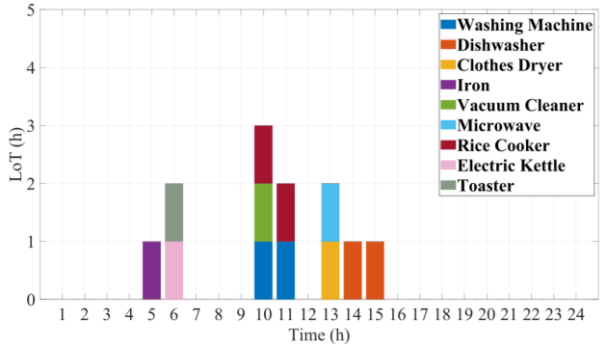


(b) Case 2

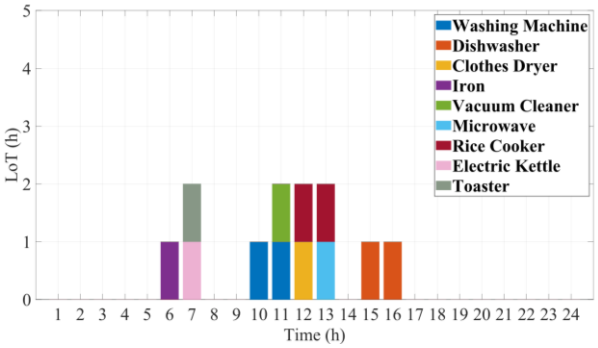


(c) Case 3

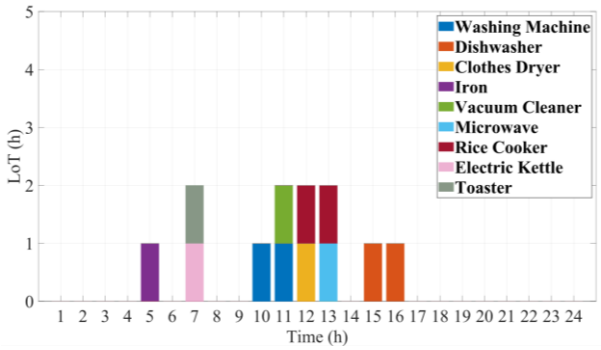


(d) Case 4

Fig. 18. The obtained scheduling for a smart home in microgrid 8.

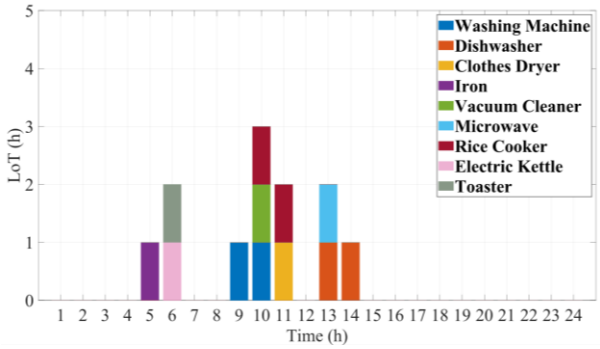


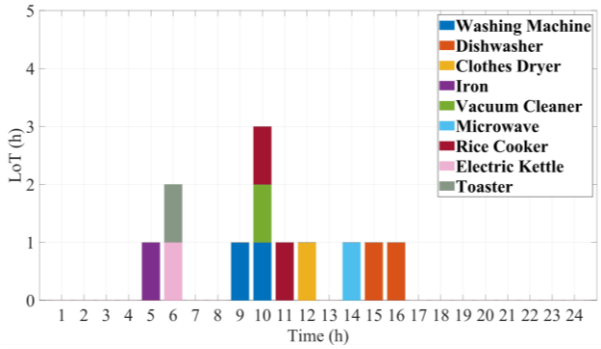

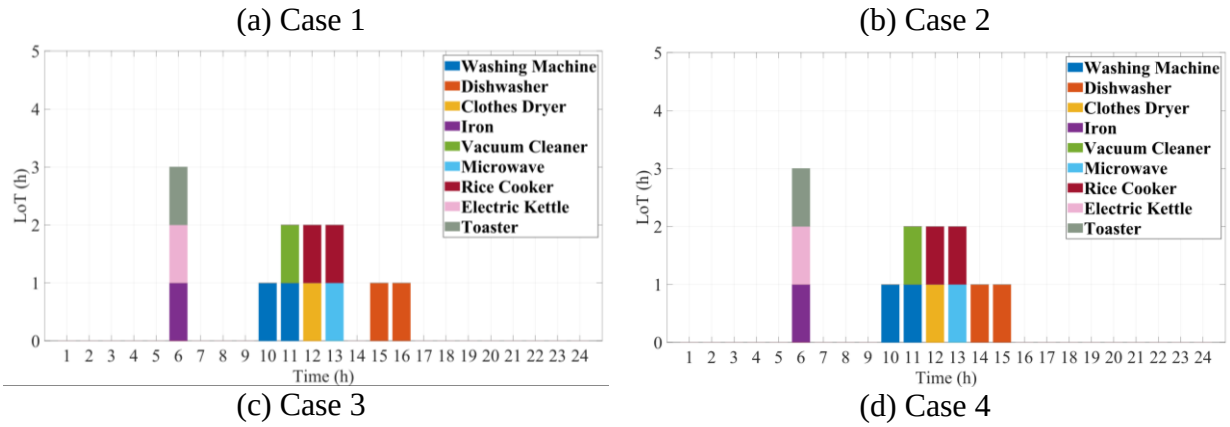


Fig. 19. The obtained scheduling for a smart home in microgrid 9.

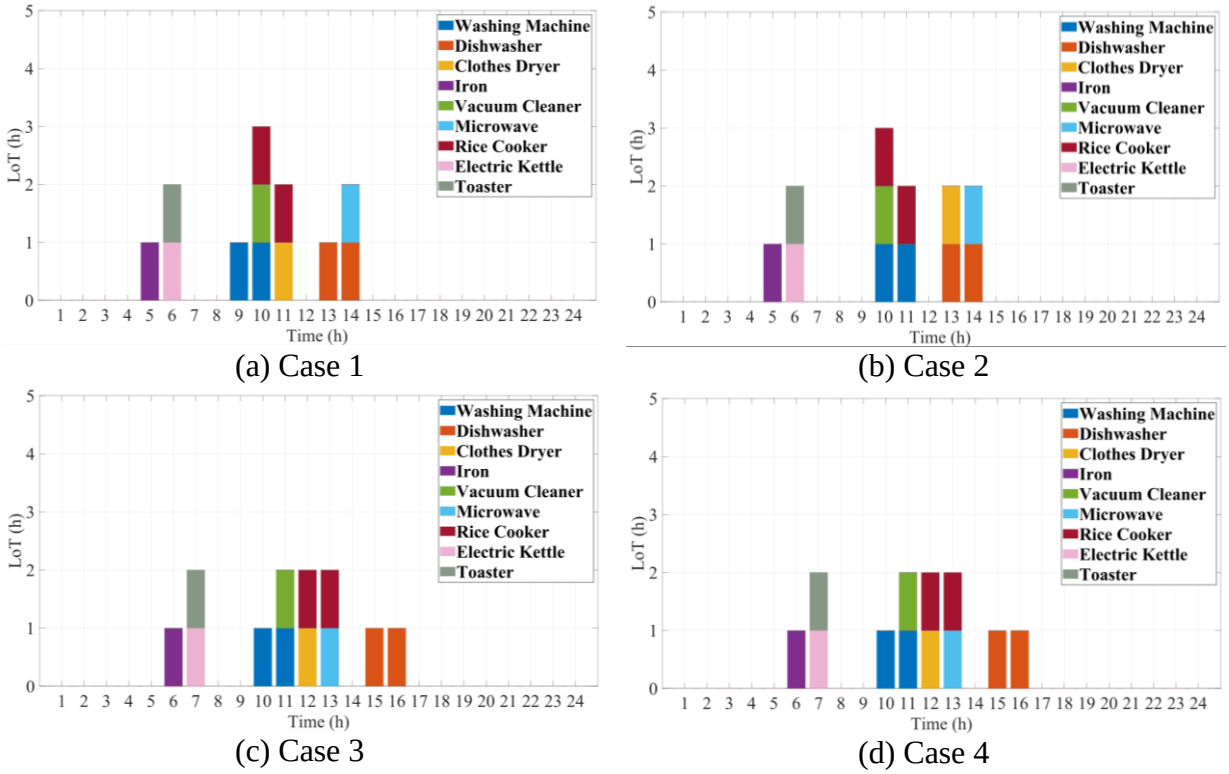


Fig. 20. The obtained scheduling for a smart home in microgrid 10.

## References

[1] Wang Y, Rousis AO, Strbac G. On microgrids and resilience: A comprehensive review on modeling and operational strategies. Renew Sustain Energy Rev 2020;134:110313. https://doi.org/https://doi.org/10.1016/j.rser.2020.110313.

[2] Chen B, Wang J, Lu X, Chen C, Zhao S. Networked Microgrids for Grid Resilience, Robustness, and Efficiency: A Review. IEEE Trans Smart Grid 2021;12:18–32.

https://doi.org/10.1109/TSG.2020.3010570.
[3] Bandeiras F, Pinheiro E, Gomes M, Coelho P, Fernandes J. Review of the cooperation and operation of microgrid clusters. Renew Sustain Energy Rev 2020;133:110311. https://doi.org/https://doi.org/10.1016/j.rser.2020.110311.
[4] Phommixay S, Doumbia ML, Lupien St-Pierre D. Review on the cost optimization of microgrids via particle swarm optimization. Int J Energy Environ Eng 2020;11:73–89. https://doi.org/10.1007/s40095-019-00332-1.
[5] Kumar KP, Saravanan B. Recent techniques to model uncertainties in power generation from renewable energy sources and loads in microgrids – A review. Renew Sustain Energy Rev 2017;71:348–58. https://doi.org/https://doi.org/10.1016/j.rser.2016.12.063.
[6] Komala K, Kumar KP, Cherukuri SHC. Storage and non-Storage Methods of Power balancing to counter Uncertainty in Hybrid Microgrids - A review. J Energy Storage 2021;36:102348. https://doi.org/https://doi.org/10.1016/j.est.2021.102348.
[7] Harsh P, Das D. Energy management in microgrid using incentive-based demand response and reconfigured network considering uncertainties in renewable energy sources. Sustain Energy Technol Assessments 2021;46:101225. https://doi.org/10.1016/j.seta.2021.101225.
[8] Adefarati T, Bansal RC. Reliability, economic and environmental analysis of a microgrid system in the presence of renewable energy resources. Appl Energy 2019;236:1089–114. https://doi.org/https://doi.org/10.1016/j.apenergy.2018.12.050.
[9] Vincent R, Ait-Ahmed M, Houari A, Benkhoris MF. Residential microgrid energy management considering flexibility services opportunities and forecast uncertainties. Int J Electr Power Energy Syst 2020;120:105981. https://doi.org/10.1016/j.ijepes.2020.105981.
[10] Leonori S, Martino A, Frattale Mascioli FM, Rizzi A. Microgrid Energy Management Systems Design by Computational Intelligence Techniques. Appl Energy 2020;277:115524. https://doi.org/https://doi.org/10.1016/j.apenergy.2020.115524.
[11] Leonori S, Paschero M, Frattale Mascioli FM, Rizzi A. Optimization strategies for Microgrid energy management systems by Genetic Algorithms. Appl Soft Comput 2020;86:105903. https://doi.org/https://doi.org/10.1016/j.asoc.2019.105903.
[12] Marino CA, Marufuzzaman M. A microgrid energy management system based on chance-constrained stochastic optimization and big data analytics. Comput Ind Eng 2020;143:106392. https://doi.org/10.1016/j.cie.2020.106392.
[13] Ding T, Lin Y, Bie Z, Chen C. A resilient microgrid formation strategy for load restoration considering master-slave distributed generators and topology reconfiguration. Appl Energy 2017;199:205–16. https://doi.org/https://doi.org/10.1016/j.apenergy.2017.05.012.
[14] Li Z, Wang S, Zhou Y, Liu W, Zheng X. Optimal distribution systems operation in the presence of wind power by coordinating network reconfiguration and demand response. Int J Electr Power Energy Syst 2020;119:105911. https://doi.org/10.1016/j.ijepes.2020.105911.
[15] Wang J, Wang W, Yuan Z, Wang H, Wu J. A Chaos Disturbed Beetle Antennae Search Algorithm for a Multiobjective Distribution Network Reconfiguration Considering the Variation of Load and DG. IEEE Access 2020;8:97392–407. https://doi.org/10.1109/access.2020.2997378.
[16] İnci M, Aygen MS. A modified energy management scheme to support phase balancing in grid interfaced photovoltaic/fuel cell system. Ain Shams Eng J 2021.

https://doi.org/https://doi.org/10.1016/j.asej.2020.12.018.
[17] Zareen N, Mustafa MW, Sultana U, Nadia R, Khattak MA. Optimal real time cost-benefit based demand response with intermittent resources. Energy 2015;90:1695–706. https://doi.org/https://doi.org/10.1016/j.energy.2015.06.126.
[18] Hafeez G, Wadud Z, Khan IU, Khan I, Shafiq Z, Usman M, et al. Efficient Energy Management of IoT-Enabled Smart Homes Under Price-Based Demand Response Program in Smart Grid. Sensors (Basel) 2020;20:3155. https://doi.org/10.3390/s20113155.
[19] ur Rehman U, Yaqoob K, Adil Khan M. Optimal power management framework for smart homes using electric vehicles and energy storage. Int J Electr Power Energy Syst 2022;134:107358. https://doi.org/10.1016/j.ijepes.2021.107358.
[20] Dey B, García Márquez FP, Basak SK. Smart Energy Management of Residential Microgrid System by a Novel Hybrid MGWOSCACSA Algorithm. Energies 2020;13:3500. https://doi.org/10.3390/en13133500.
[21] Rocha HRO, Honorato IH, Fiorotti R, Celeste WC, Silvestre LJ, Silva JAL. An Artificial Intelligence based scheduling algorithm for demand-side energy management in Smart Homes. Appl Energy 2021;282:116145. https://doi.org/10.1016/j.apenergy.2020.116145.
[22] Wang J, Liu J, Li C, Zhou Y, Wu J. Optimal scheduling of gas and electricity consumption in a smart home with a hybrid gas boiler and electric heating system. Energy 2020;204:117951. https://doi.org/https://doi.org/10.1016/j.energy.2020.117951.
[23] Behzadi A, Arabkoohsar A. Feasibility study of a smart building energy system comprising solar PV/T panels and a heat storage unit. Energy 2020;210:118528. https://doi.org/https://doi.org/10.1016/j.energy.2020.118528.
[24] Nikmehr N. Distributed robust operational optimization of networked microgrids embedded interconnected energy hubs. Energy 2020;199:117440. https://doi.org/https://doi.org/10.1016/j.energy.2020.117440.
[25] Tan B, Chen H. Multi-objective energy management of multiple microgrids under random electric vehicle charging. Energy 2020;208:118360. https://doi.org/https://doi.org/10.1016/j.energy.2020.118360.
[26] Safaie AA, Alizadeh Bidgoli M, Javadi S. A multi-objective optimization framework for integrated electricity and natural gas networks considering smart homes in downward under uncertainties. Energy 2022;239:122214. https://doi.org/https://doi.org/10.1016/j.energy.2021.122214.
[27] Alizadeh Bidgoli M, Ahmadian A. Multi-stage optimal scheduling of multi-microgrids using deep-learning artificial neural network and cooperative game approach. Energy 2022;239:122036. https://doi.org/https://doi.org/10.1016/j.energy.2021.122036.
[28] Mukhopadhyay B, Das D. Multi-objective dynamic and static reconfiguration with optimized allocation of PV-DG and battery energy storage system. Renew Sustain Energy Rev 2020;124:109777. https://doi.org/10.1016/j.rser.2020.109777.
[29] Guo S, Lin J, Zhao Y, Wang L, Wang G, Liu G. A Reliability-Based Network Reconfiguration Model in Distribution System with DGs and ESSs Using Mixed-Integer Programming. Energies 2020;13. https://doi.org/10.3390/en13051219.
[30] Kahouli O, Alsaif H, Bouteraa Y, Ben Ali N, Chaabene M. Power System Reconfiguration in Distribution Network for Improving Reliability Using Genetic Algorithm and Particle Swarm Optimization. Appl Sci 2021;11. https://doi.org/10.3390/app11073092.
[31] Xu X, Hu W, Liu W, Du Y, Huang R, Huang Q, et al. Risk management strategy for a

renewable power supply system in commercial buildings considering thermal comfort and stochastic electric vehicle behaviors. Energy Convers Manag 2021;230:113831. https://doi.org/10.1016/j.enconman.2021.113831.
[32] Akter MN, Mahmud MA, Haque ME, Oo AMT. An optimal distributed energy management scheme for solving transactive energy sharing problems in residential microgrids. Appl Energy 2020;270:115133. https://doi.org/10.1016/j.apenergy.2020.115133.
[33] Nunna HSVSK, Sesetti A, Rathore AK, Doolla S. Multiagent-Based Energy Trading Platform for Energy Storage Systems in Distribution Systems With Interconnected Microgrids. IEEE Trans Ind Appl 2020;56:3207–17. https://doi.org/10.1109/tia.2020.2979782.
[34] Haseeb M, Kazmi SAA, Malik MM, Ali S, Bukhari SBA, Shin DR. Multi Objective Based Framework for Energy Management of Smart Micro-Grid. IEEE Access 2020;8:220302–19. https://doi.org/10.1109/access.2020.3041473.
[35] Violante W, Canizares CA, Trovato MA, Forte G. An Energy Management System for Isolated Microgrids With Thermal Energy Resources. IEEE Trans Smart Grid 2020;11:2880–91. https://doi.org/10.1109/tsg.2020.2973321.
[36] Alhasnawi BN, Jasim BH, Rahman Z-ASA, Siano P. A Novel Robust Smart Energy Management and Demand Reduction for Smart Homes Based on Internet of Energy. Sensors (Basel) 2021;21:4756. https://doi.org/10.3390/s21144756.
[37] Jiménez M, Bilbao A. Pareto-optimal solutions in fuzzy multi-objective linear programming. Fuzzy Sets Syst 2009;160:2714–21. https://doi.org/10.1016/j.fss.2008.12.005.
[38] Yuan H, Li F, Wei Y, Zhu J. Novel linearized power flow and linearized OPF models for active distribution networks with application in distribution LMP. IEEE Trans Smart Grid 2018;9:438–48. https://doi.org/10.1109/TSG.2016.2594814.
[39] Haghighat H, Zeng B. Distribution System Reconfiguration under Uncertain Load and Renewable Generation. IEEE Trans Power Syst 2016;31:2666–75. https://doi.org/10.1109/TPWRS.2015.2481508.
[40] Mansouri SA, Ahmarinejad A, Nematbakhsh E, Javadi MS, Jordehi AR, Catalão JPS. Energy Management in Microgrids including Smart Homes: A Multi-objective Approach. Sustain Cities Soc 2021:102852. https://doi.org/https://doi.org/10.1016/j.scs.2021.102852.
[41] Eladl AA, El-Afifi MI, Saeed MA, El-Saadawi MM. Optimal operation of energy hubs integrated with renewable energy sources and storage devices considering CO2 emissions. Int J Electr Power Energy Syst 2020;117:105719. https://doi.org/10.1016/j.ijepes.2019.105719.
[42] Amir Mansouri S, Javadi MS, Ahmarinejad A, Nematbakhsh E, Zare A, Catalão JPS. A coordinated energy management framework for industrial, residential and commercial energy hubs considering demand response programs. Sustain Energy Technol Assessments 2021;47:101376. https://doi.org/10.1016/j.seta.2021.101376.
[43] Bui VH, Hussain A, Kim HM. A multiagent-based hierarchical energy management strategy for multi-microgrids considering adjustable power and demand response. IEEE Trans Smart Grid 2018;9:1323–33. https://doi.org/10.1109/TSG.2016.2585671.
[44] Wan J, Zheng F, Luan H, Tian Y, Li L, Ma Z, et al. Assessment of wind energy resources in the urat area using optimized weibull distribution. Sustain Energy Technol Assessments 2021;47:101351. https://doi.org/https://doi.org/10.1016/j.seta.2021.101351.

[45] Newlun CJ, McCalley JD, Amitava R, Ardakani AJ, Venkatraman A, Acevedo ALF-. Adaptive Expansion Planning Framework for MISO Transmission Planning Process. 2021 IEEE Kansas Power Energy Conf., 2021, p. 1–6. https://doi.org/10.1109/KPEC51835.2021.9446221.
[46] Alabedin AMZ, El-Saadany EF, Salama MMA. Generation scheduling in Microgrids under uncertainties in power generation. 2012 IEEE Electr. Power Energy Conf., 2012, p. 133–8. https://doi.org/10.1109/EPEC.2012.6474937.
[47] Zhang D, Fu Z, Zhang L. An improved TS algorithm for loss-minimum reconfiguration in large-scale distribution systems. Electr Power Syst Res 2007;77:685–94. https://doi.org/10.1016/j.epsr.2006.06.005.